SAE The Engineering Society For Advancing Mobility Land Sea Air and Space®
INTERNATIONAL
400 Commonwealth Drive, Warrendale, PA 15096-0001

SURFACE VEHICLE INFORMATION REPORT

An American National Standard

SAE J2071

REV. JUN94

Issued 1990-03
Revised 1994-06

Superseding J2071 MAR90

AERODYNAMIC TESTING OF ROAD VEHICLES - OPEN THROAT WIND TUNNEL ADJUSTMENT

***Foreword*—**This document has also changed to comply with the new SAE Technical Standards Board format. The document title has also changed.

***1. Scope*—**As a simulation of road driving, wind tunnel testing of full-size vehicles produces certain errors in the aerodynamic forces, aerodynamic moments, and surface pressures. The magnitude of these errors, in general, depends on the following:

a. Flow quality
b. Determination of the reference dynamic pressure
c. Wind tunnel floor boundary layer
d. Test section geometry and position of the car within that geometry
e. Shape of the vehicle
f. Blockage ratio: The ratio of the cross-sectional area of the vehicle to the cross-sectional area of the wind tunnel nozzle
g. Wheel rotation
h. Internal flow in the model

The SAE Standards Committee, Open Throat Wind Tunnel Adjustments had as a goal to document the knowledge of the influence of model interference on wind tunnel test results for automotive open jet wind tunnels. This document contains the following information related to this subject:

a. Design data of open throat wind tunnels
b. A summary of published and unpublished test data
c. Documentation and theoretical explanation of various blockage correction procedures for automotive tests
d. Critical evaluation of blockage correction procedures, especially in relation to other influences, such as test section geometry, position of the car, floor boundary layer, etc.
e. Recommendation of a calibration procedure to determine the effect of blockage and other influences in each individual wind tunnel

An initial goal of the committee, to recommend a well proven correction procedure for automotive open jet wind tunnels based on blockage theory (Figure 1), could not be established at this time. The reason is that, besides blockage, other factors, such as test section geometry, are at least as influential as pure blockage. As these influential parameters are wind tunnel specific, a general valid adjustment procedure is presently not available.

QUESTIONS REGARDING THIS DOCUMENT: (724) 772-8512 FAX: (724) 776-0243
TO PLACE A DOCUMENT ORDER; (724) 776-4970 FAX: (724) 776-0790
SAE WEB ADDRESS http://www.sae.org

Clean Blockage means:

- ○ no boundary layer effects
- ○ no nozzle effects
- ○ no collector/model interaction
- ○ no buoyancy effects (i.e. longitudinal static pressure gradient)

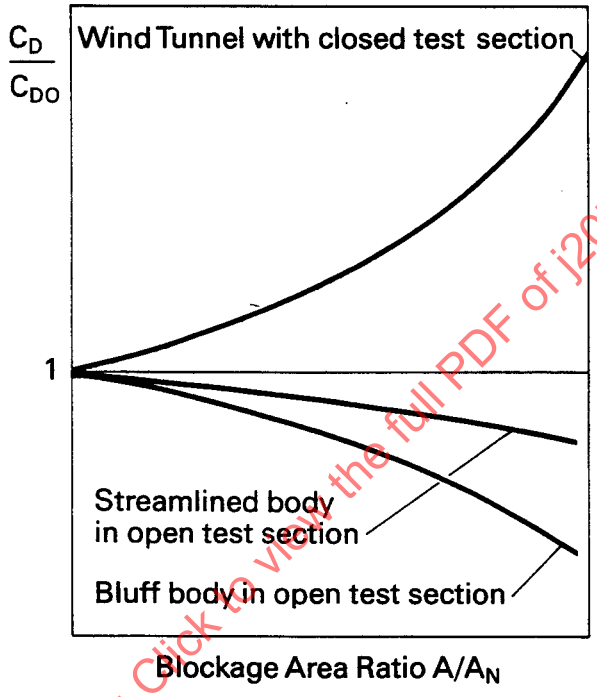

FIGURE 1—PURE MODEL SIZE INFLUENCE

2. References

2.1 Applicable Publications—The following publications form a part of the specification to the extent specified herein. Unless otherwise indicated the lastest revision of SAE publications shall apply.

2.1.1 SAE PUBLICATIONS—Available from SAE, 400 Commonwealth Drive, Warrendale, PA 15096-0001.

1. Ludvigsen, K.E.
Automotive Aerodynamic Research Over Past 50 Years in Germany, Great Britain, Italy, United States, and Other Countries
SAE Paper 700035, 1970
2. Buchheim, R. et al.
Comparison Tests Between Major European Automotive Wind Tunnels.
SAE Paper 800140, Detroit, 1980
3. Buchheim, R. et al.
Comparison Tests Between Major European and North American Automotive Wind Tunnels
SAE Paper 830301, Detroit, 1983

4. Cogotti, A. et al.
Comparison Test Between Some Full-Scale European Automotive Wind Tunnels - Pininfarina Reference Car
SAE Paper 800139, Detroit, 1980
5. Costelli, A. et al.
FIAT Research Center Reference Car: Correlation Tests Between Four Full Scale European Wind Tunnels and Road
SAE Paper 810187, Detroit, 1981
6. Carr, G.W., Stapleford, W.R.
Blockage Effects in Automotive Wind-Tunnel Testing
SAE Paper 860093/1986
7. Mercker, E.
General Consideration About Blockage Correction in Open Jet Wind Tunnels
SAE Subcommittee No. 9 - Communication (1987)
8. Janssen, L.J., Domeland, P., Lindener, N.
The New BMW Acoustic Wind Tunnel
Paper planned for SAE Congress, Detroit, February 1990
9. Janssen, L.J., Lindener, N., Mullenbach, P., VAGT, J.-D.
Measurement of Tunnel Speed and Static Reference Pressure in Open Jet Automotive Wind Tunnels
Paper planned for SAE Congress, Detroit, February 1990

2.1.2 Other Publications

1. Konig-Fachsenfeld, R.
Aerodynamik des Kraftfahrzeugs Umschau-Verlag, Frankfurt a.M.
2. Kramer, C. et al.
Wind Tunnels for Industrial Aerodynamics
J. Wind Engineering and Industrial Aerodynamics 16 (1984), pp 225–264
3. Lock, C.N.H.
The Interference of a Wind Tunnel on a Symmetrical Body
ARC, R & M 1275, 1929
4. Wust, W.
Verdrängungskorrektur für rechteckige Windkanäle bei verschiedenen Strahlbegrenzungen und bei exzentrischer Lage des Modells
Z. Flugwiss. 9 (1961), p. 15
5. Schulz, G.
Die Verdrängungskorrekturen in Unterschallwindkanälen und die Grenzen ihrer Anwendbarkeit
Z. Flugwiss. 20 (1972), p. 261
6. Kuchemann, D., Vandrey, F.
Zur Geschwindigkeitskorrektur in Windkanälen mit freier Meβstrecke unter besonderer Berücksichtigung des Düseneinflusses
Jahrb. 1941 der deutschen Luftfahrtforschung
7. Mercker, E.
A Blockage Correction for Automotive Testing in a Wind Tunnel With Closed Test Section
J. Wind Engineering and Industrial Aerodynamics, 22 (1986)
8. Maskell, E.
A Theory of the Blockage Effects on Bluff Bodies and Stalled Wings in a Closed Wind Tunnel
ARC, R & M 3400, 1961
9. Sachs, P.
Wind Forces in Engineering
Pergamon Press, Volume 3, 1972
10. Rogers, E.
Subsonic Wind Tunnel Wall Corrections
AGARDograph 109, 1966

11. Owen, T.B.
Measured Blockage Effects on Bluff Bodies in Closed and Open Wind Tunnels
RAE Technical Report 78151, Dec. 1978, London
12. Templin, J.T., Raimondo, S.
Experimental Evaluation of Test Section Boundary Interference Effects in Road Vehicle Tests in Wind Tunnels
6th Colloquium on Industrial Aerodynamics, June 19–21, 1985, Aachen
13. Gerhardt, H.J., KRAMER, C.
Blockierungseffekte in Windkanälen mit Bodenplatte und offener Meβstrecke Vortrag im HDT im Rahmen des Seminars
Kraftfahrzeugaerodynamik, 11/87
14. Mercker, E.
Eine Blockierungskorrektur für aerodynamische Messungen in offenen und geschlossenen Unterschallwindkanälen, Doctorate
Thesis, Dec. 1980, Berlin
15. Cooper, K.R., et al.
A Comparison of Aerodynamic Drag Measurements on Model Trucks in Closed Jet and Open Jet Wind Tunnels
6th Colloquium on Industrial Aerodynamics, June 19–21, 1985, Aachen
16. Garner, H.C., et al.
Subsonic Wind Tunnel Wall Corrections
AGARDograph 109, Oct. 1966
17. Frimberger, R., Pucher, P.
Ringversuche zur Klärung des Versperrungseinflusses kantiger Körper in Windkanälen mit offener Meβstrecke
Institut für Strömungsmechanik, TU München, Bericht 77/1
18. Regenscheit, B.
Isotherme Luftstrahlen, Verlag C.F.
Müller, Karlsruhe 1981
19. Kramer, C. et al.
Auslegung von Freistrahlmeβstrecken für Fahrzeugwindkanäle
Vortrag im HDT im Rahmen des Seminars
Aerodynamik von Kraftfahrzeugen, 11/87
20. Kramer, C., Gerhardt, H.J., Janssen, L.J.
Flow Studies of an Open Jet Wind Tunnel and Comparison With Closed and Slotted Walls
Journal of Wind Engineering and Industrial Aerodynamics, 22 (1986), 115–127
21. V. Schulz-Hausmann, F.K., Vagt, J.-D.
Influence of Test Section Length and Collector Area on Measurements in Three-Fourths Open Jet in Automotive Industry
SATA-Conference No. 23, Palo Alto, CA, 1987
22. Vagt, J.-D.
Merkmale des Porsche-Meβzentrums für Aerodynamik
Haus der Technik Tagung Nr. T-30-905-056-7, Nov. 1987
23. Mullenbach, P., Deutenbach, K.-R.
Determination of Dynamic Pressure and Reference Pressure in Automobile Wind Tunnels With Open Test Sections
8th Colloquium on Industrial Aerodynamics, Aachen, 4–7 Sept. 1989

3. Description of Open Jet Automotive Wind Tunnels—For automotive applications, an open jet wind tunnel is a wind tunnel where the test section is three-fourths open and the road is represented by a level floor. For historical reasons (2.1.1 (1) and 2.1.2 (1)), open jet wind tunnels for automotive testing are used mainly in Europe. Their principal advantages are as follows:

a. Theoretically lower absolute values of blockage correction compared to closed test sections
b. Easy access to the test section

In designing open jet wind tunnels, the control of the flow quality data is a major problem. Based on the available data and the experience of the members of the committee, the flow quality data that are generally sufficient, and (in any case) achievable, in an open jet wind tunnel for automotive testing are given in Table 1.

TABLE 1—FLOW QUALITY FOR OPEN THROAT TEST SECTIONS - EXISTING MINIMUM REQUIREMENT

		Existing Minimum Requirement
Angularity in pitch	$\Delta\alpha$ (deg)	$\leq \pm 0.5$
Angularity in yaw	$\Delta\beta$ (deg)	$\leq \pm 0.5$
Uniformity of flow velocity	Δv (%)	$\leq \pm 1.0$
Turbulence intensity	Tux (%)	≤ 0.5
Pressure Level variation	Δcp (-)	< 0.01
Length of pressure level	$\Delta 1/L$ (-)	≥ 1.0 (≥ 1.5) (1)
Displacement thickness	δ^* (mm)	10% of the ground clearance

1. Some experimental results (Vagt SAE 88) suggest that for larger blockage ratios (>5% – 10%) the length of constant pressure level should be increased.

The test section geometrical parameters of various open jet wind tunnels used for full-scale automotive testing are given in Table 2. Table 3 gives the data for tunnels that are used for scale model testing. The effect of these geometrical parameters is superimposed on blockage effects in open jet wind tunnels, as will be shown later.

TABLE 2—OPEN TEST SECTION GEOMETRY OF LARGE TUNNELS (FOR FULL-SCALE TESTING)

WT Owner / WT Part	Dimension	BMW AE	BMW AC	DB	FIAT	FORD	PININF.	PORSCHE	VW	IVK
Nozzle Exit Area	m^2	20.02	10.0	32.64	30.0	23.75	11.75	22.3	37.5	22.45
Nozzle Width	m	5.77	4.0	7.4	7.0	6.0	5.0	6.2	7.5	5.8
Nozzle Height	m	3.47	2.828	4.9	4.6	4.0	2.9	3.6	5.0	3.87
Nozzle Contraction Ratio	-	3.66	3.0	3.6	4.0	4.0	6.5	6.06	4.0	4.411
Test Section Length	m	10.02	9.83	10.0	10.5	10.5	8.0	13.5	10.0	9.5
T-S Surr. Bound. Width	m	10.34	13.74	14.8	12.2	15.0	9.6	12.7	17.0	15.0
T-S Surr. Bound. Height	m	5.30	5.72	7.5	10.8	8.5	4.2	6.85	13.0	8.5
Model. Ref. Point x/L (TS)	-	0.471	0.356	0.5	0.55	0.39	0.46	0.41	0.43	0.474
Collector Cross Section	m^2	22.12	22.64	47.4	40.5	29.73	17.33	42.2	44.8	26.5
Collector Width	m	6.01	5.66	8.5	7.8	6.68	6.2	8.7	8.0	6.354
Collector Height	m	3.68	4.0	6.5	5.6	4.45	3.5	4.85	5.6	4.166
Maximum Speed	m/s	50	70	70	56	51	54	64	50	75

TABLE 3—OPEN TEST SECTION GEOMETRY OF SMALL TUNNELS (FOR SCALE MODEL TESTING)

WT Owner / WT Part	Dimension	Aachen	Aachen	DB	DLR	DLR	DLR	FIAT	FORD	IVK	PORSCHE	VOLVO	VW
Nozzle Exit Area	m^2	1.0	2.69	1.64	8.61	8.1	1.53	4.0	8.64	1.654	1.4	4.125	6.0
Nozzle Width	m	1.1	2.0	1.5	3.25	3.0	1.3	2.4	3.65	1.575	1.55	2.4	3.0
Nozzle Height	m	1.1	1.4	1.096	2.65	2.7	1.18	1.7	2.44	1.05	0.9	1.73	2.0
Nozzle Contraction Ratio	-	3.3	2.57	6.0	5.6	5.44	4.91	7.0	11.0	4.988	6.06	6.25	6.0
Test Section Length	m	1.83	4.0	2.8	6.0	6.0	2.48	4.0	6.1	2.578	3.38	8.82	6.0
T-S Surr. Bound. Width	m	8.65	5.74	5.15	16.4	8.0	4.8	5.7	15.0	6.85	3.42	6.06	6.5
T-S Surr. Bound. Height	m	4.0	2.85	2.35	9.5	5.9	5.2	6.4	8.5	3.39	1.84	4.0	4.0
Model Ref. Point x/L (TS)	-	0.55	0.38	0.46	0.43	0.48	0.5	0.4	0.41	0.474	0.41	0.283	0.42
Collector Cross Section	m^2	1.45	4.2	2.3	10.26	17.0	1.84	7.6	11.33	1.921	2.66	12.25	6.9
Collector Width	m	1.32	2.4	1.85	3.67	5.15	1.5	3.3	4.12	1.712	2.18	3.5	3.0
Collector Height	m	1.32	1.7	1.3	2.8	3.3	1.28	2.3	2.75	1.122	1.22	3.5	2.3
Maximum Speed	m/s	42	38	65	75	65	55	70	84	80	64	53	50

The data given in Tables 1, 2, and 3 are also an indication of the range of flow quality and test section design data for which the following discussions about blockage corrections are valid. The data are based on the present experience of the committee members. The definition of the various values is as follows:

a. Standard Control Box Test Volume: All flow quality parameters will be related to a standard control box test volume. The test vollume size is defined as:

Length = 100% of typical vehicle length
Height = 100% of typical vehicle height
Width = 100% of typical vehicle width for nonyawed conditions
= 200% of typical vehicle width for yawed conditions

b. Angularity in Flow Direction: The angularity in pitch, $\Delta\alpha$, is the maximum tolerable local deviation of flow pitch angle in a control volume. It is defined as the angle between the flow direction and the x-axis of the ground plane (x-y-plane), positive for upward incident flow. The angularity in yaw, $\Delta\beta$, is the maximum tolerable local deviation of flow yaw angle in a control volume. It is defined as the angle between the flow direction and the x-axis in the vertical x-z-plane, positive for incident flow from left to right (looking upstream).

c. Uniformity of Flow Velocity: The uniformity of flow velocity, $\Delta V = (V\text{-}V\infty)/V\infty$, is given in percent, ΔV is the maximum tolerable flow velocity deviation in a control volume, with V as local stream wise velocity, except in boundary layer regions, and $V\infty$ as the magnitude of the total relative airflow vector.

d. Turbulence Intensity: Tu_x is the maximum tolerable turbulence intensity in the stream wise direction in a control volume.

e. Constant Pressure Conditions: The maximum tolerable local static pressure deviation is $\Delta c_p = (p\text{-}\overline{p\infty})/q\infty$, where $\overline{p\infty}$ denotes the mean value in the region from car front to base plane.
The length of this "constant" pressure plateau in the test section, $\Delta 1$, is related to the car length L. Constant means that the pressure deviation is less than, or equal to, ΔC_p.

f. Displacement Thickness:

$$\delta^* = \int_{\infty}^{\infty} (1 - V/V\infty)\,dy \qquad \text{(Eq. 1)}$$

is the maximum tolerable displacement thickness at the origin of the coordinate system (in general, the center of the balance) with a stream velocity $V\infty$ = 140 km/h and no car in the test section.

4. Literature Survey of Open Jet Automotive Wind Tunnels - Model Interference—By far, the majority of the papers on blockage effects in wind tunnels are concerned with closed test sections. Only a few papers present theoretical investigations on the blockage in open jet wind tunnels. The experimental papers (2.1.1 (2) to 2.1.1 (6) and 2.1.2 (2)) do not distinguish between blockage and other parameters influencing measurement. Therefore, the results are rather inconclusive and show mainly that each wind tunnel has its own wind tunnel specific behavior, which is related both to the boundary condition consequent on the tunnel (test section) design and to blockage.

4.1 Theoretical/Semitheoretical Approaches—In the case of solid blockage, the theoretical investigations on open wind tunnel blockage are based on the work of Lock (see 2.1.2 (3)). Lock considered the velocity difference in the test section due to the model and derived the equation:

$$\Delta V/V\infty = \tau\ \lambda\ (A/A_N)3/2 \qquad \text{(Eq. 2)}$$

where:

ΔV = velocity difference due to blockage
τ = test section boundary specific blockage coefficient
λ = model specific coefficient
A = maximum model cross-sectional area
A_N = wind tunnel cross section

The change in the drag is related to the velocity difference.

$$D_m/D_\infty = (1 + (\Delta V/V_\infty))\ \ 2 \sim 1 + 2\ (\Delta V/V_\infty) \qquad \text{(Eq. 3)}$$

where:

D_m = measured drag
D_∞ = drag in unconfined flow

For the mathematical approach, which is based on the method of mirror imaging, Lock approximated the test section by a flow with the cross section of the wind tunnel nozzle with infinite length. The model is represented by a doublet producing the same velocity field at a large distance. The straight and parallel test section boundaries are simulated by double, infinite rows of doublets of equal strength. For a solid wall these doublets have the same sign as the doublet in the test section. For free boundaries, e.g., an open jet wind tunnel, the sign is reversed.

Based on Lock's theory, Wüst (see 2.1.2 (4)) has calculated blockage corrections for wind tunnels with rectangular cross sections and various test section boundaries. Wüst carried out the calculations for central and eccentric positions of the model. The model itself was simulated, as in Lock's work, by a doublet. The blockage correction factor is, therefore, related to the center point of the model only.

Figure 2 gives a summary of the most important results of Wüst's calculations. Shown is the test section boundary coefficient τ versus aspect ratio, H_T/B_T, of a rectangular test section with different test section boundary conditions. Lock derived information about the model specific coefficient λ. Figure 3 shows λ versus the slenderness, L/D, for bodies of revolution with different curvature.

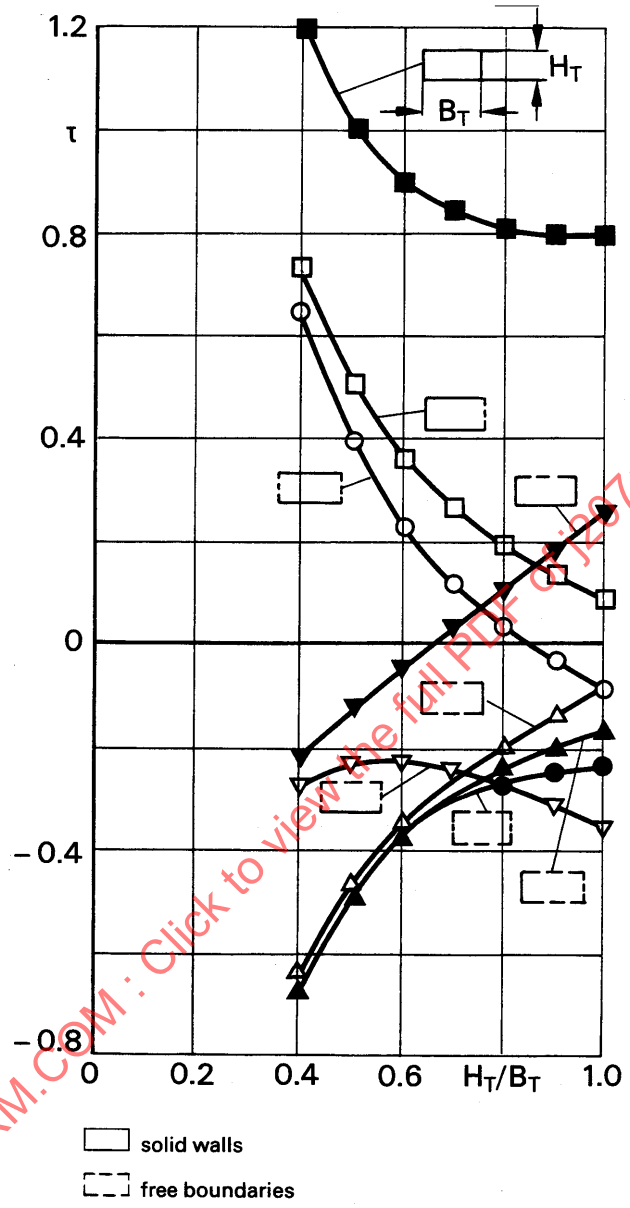

FIGURE 2—TEST SECTION BOUNDARY FACTOR τ (WIND TUNNEL FACTOR) AS A FUNCTION OF THE CROSS SECTION RATIO FOR VARIOUS BOUNDARIES AFTER REFERENCE 2.1.2 (4), MODEL PLACED IN CENTERLINE

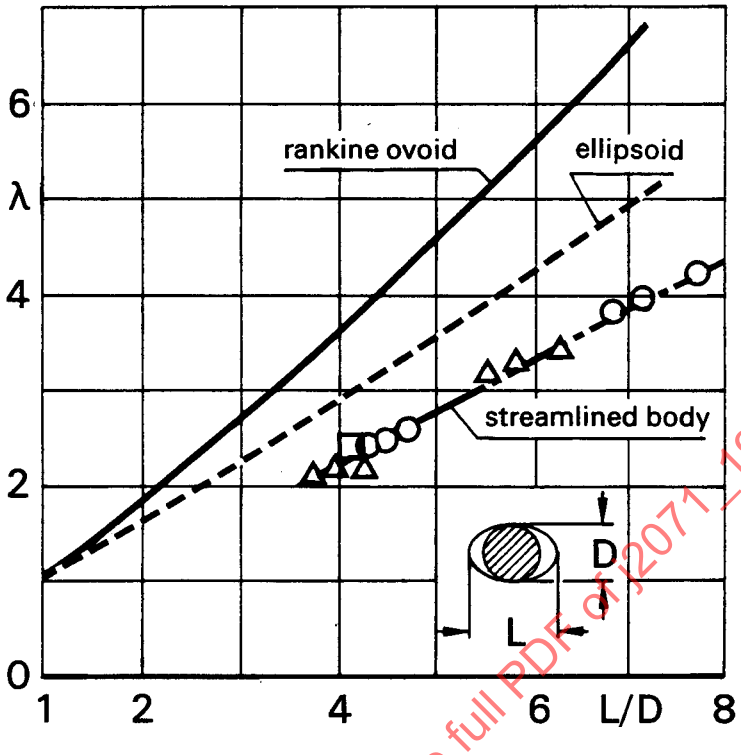

FIGURE 3—MODEL SHAPE FACTOR λ AS A FUNCTION OF RELATIVE THICKNESS FOR VARIOUS BODIES OF REVOLUTION AFTER REFERENCE 2.1.2 (4), MODEL PLACED IN CENTERLINE

The information presented in Figures 2 and 3 is valid for a model centered in the test section. Figure 4 shows results of calculations by Wüst for a model position vertically eccentric in an open test section with ground plate.

Considering the car only in such three-fourths open test sections, the eccentricity of the model is in the range of $-0.75 \leq E/H_T \leq -0.5$, leading to test section boundary coefficients $-1 > \tau > -8$, but in car aerodynamics the ground plate representing the road surface belongs to the model. Therefore, it is necessary to substitute the original test condition, i.e. a model near to a boundary of the jet by a system where the test section is imaged at the ground plate. Now the model and also the ground plate are centered. In the new system, the height is equal to the width of the original one and the new width is twice the old height. Under these circumstances the aspect ratio is in the region of 0.7, leading to $\tau = +0.85$ for the closed test section and $\tau = -0.3$ for the open test section.

Whereas Wüst calculated the test section boundary coefficient τ only for the location of the model center, Schulz (see 2.1.2 (5)) extended Wüst's considerations and included the variation of the blockage factor τ over the whole cross section of the test section for centered and for eccentric model position. Schulz calculated the distribution of the pertubation velocities over the whole cross section. Thus, he could show the difference between the model centerline and a point on the model surface, assuming for the model a simple body of revolution. From the nonhomogeneous velocity distribution, Schulz calculated correction factors for the test section dynamic pressure. Figure 5 shows the dynamic pressure correction factor versus blockage for a rectangular closed test section and an open jet test section with aspect ratio $H_T/B_T = 0.7$. For blockage ratios $A/A_N > 0.05$, the difference between model centerline and circumference becomes noticeable.

The above mentioned investigations are valid only for bodies of revolution situated far from the regions of influence of the nozzle and the collector, in the case of a real wind tunnel. Küchemann and Vandrey (see 2.1.2 (6)) have investigated how the velocity upstream of a model changes with distance from the nozzle. The investigation was carried out for bodies described by a doublet and for spheres, in open jet wind tunnels and closed wind tunnels. The results are presented in Figures 6 and 7. Given are the perturbation velocities as a function of model to nozzle distance.

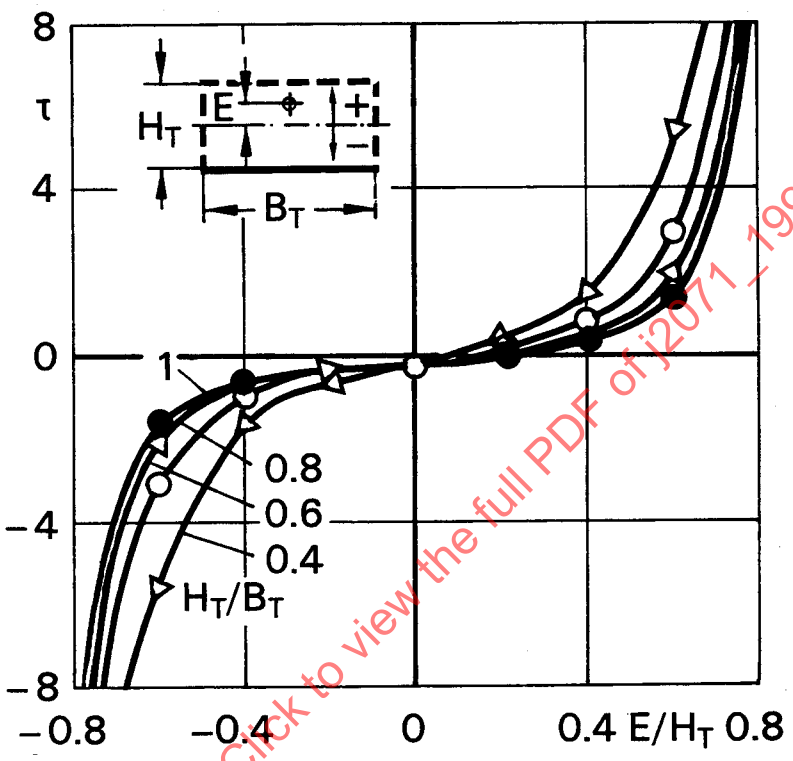

FIGURE 4—DISPLACEMENT CORRECTION FOR THREE-FOURTHS OPEN WIND TUNNEL AT VARIOUS CROSS SECTION ASPECT RATIOS AND ECCENTRICAL MODEL POSITION AFTER REFERENCE 2.1.2 (5)

To summarize the various parameters influencing the flow around a model in an open automotive wind tunnel, which normally are attributed to wind tunnel blockage:

a. The shape of the cross section (aspect ratio) and position of the model reference point in the cross section (eccentricity) (Figures 2 and 4)
b. Shape of the model (Figure 3)
c. Spatial extension of the model at nonsymmetrical model positions (Figures 4 and 5)
d. Distance between model and nozzle and model and collector, respectively, related to the model length (Figures 6 and 7)

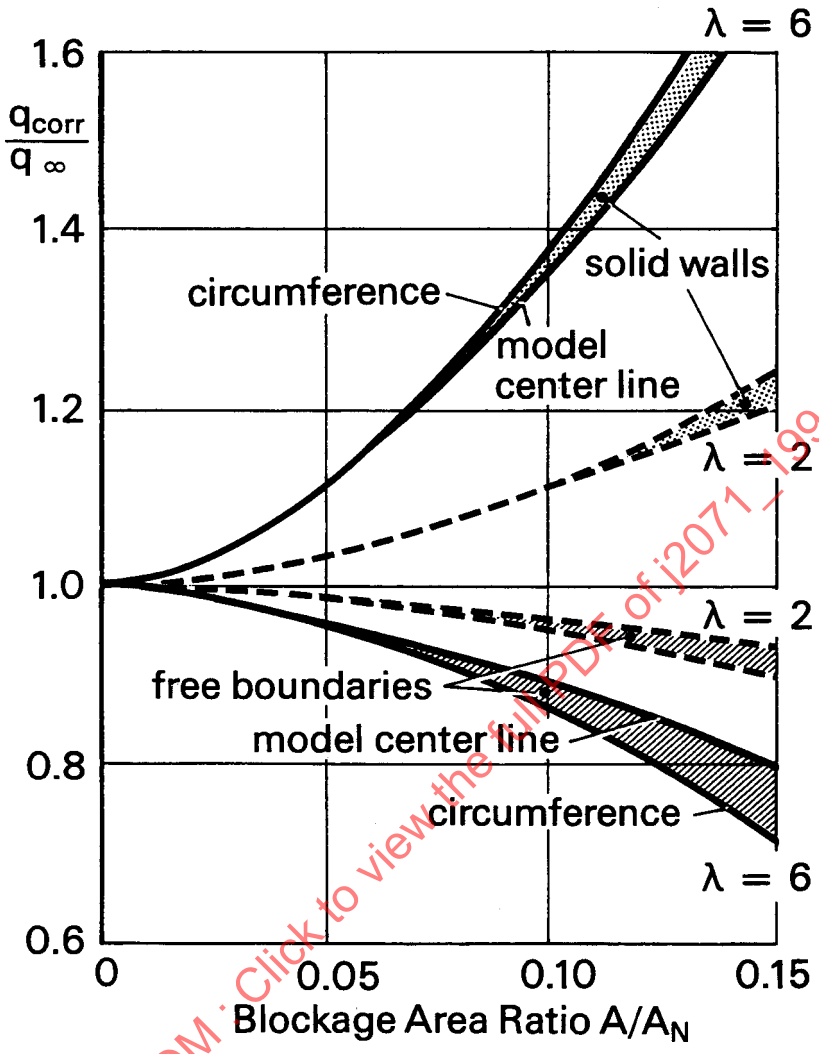

FIGURE 5—DYNAMIC PRESSURE CORRECTION AS A FUNCTION OF BLOCKAGE AREA RATIO AT CLOSED AND OPEN TEST SECTIONS FOR CENTRIC MODEL POSITION AFTER REFERENCE 2.1.2 (5)

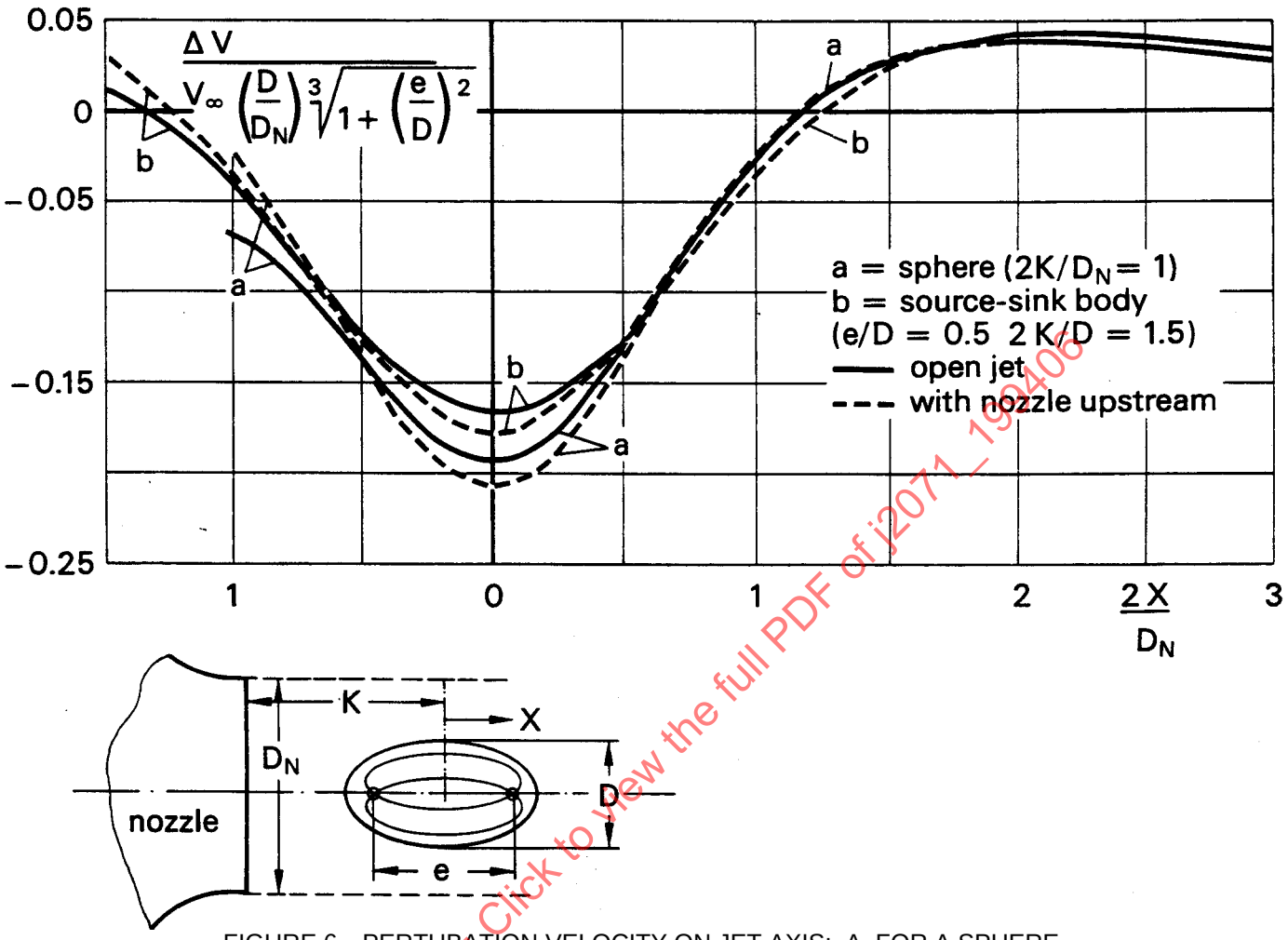

FIGURE 6—PERTUBATION VELOCITY ON JET AXIS: A. FOR A SPHERE
B. FOR A SOURCE SINK BODY AFTER REFERENCE 2.1.2 (6)

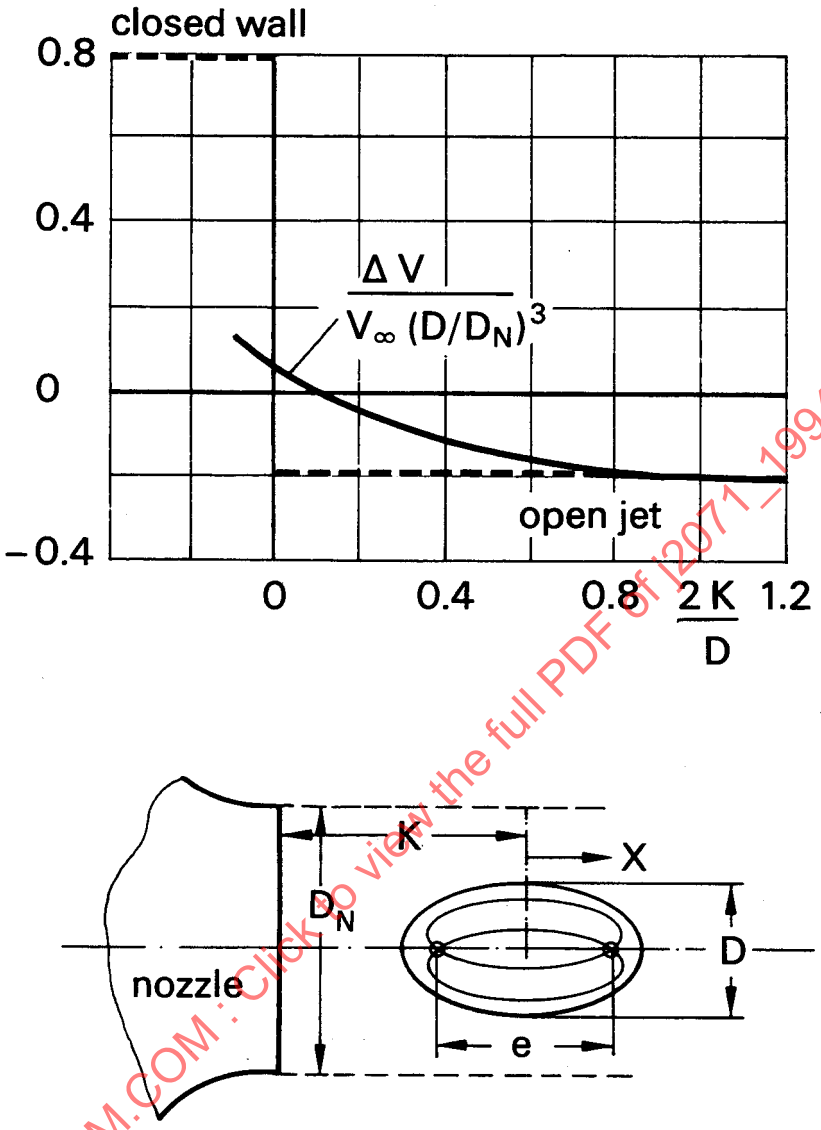

FIGURE 7—PERTUBATION VELOCITY IN THE CENTER OF A SPHERE VERSUS DISTANCE TO NOZZLE AFTER REFERENCE 2.1.2 (6)

Mercker (see 2.1.1 (7)) suggested a blockage correction for automotive testing in open jet wind tunnels. He assumed that the blockage can be assigned to three main causes:

a. Solid blockage effects
b. Wake blockage effects
c. Horizontal buoyancy effects, which can be ascribed to blockage only in an indirect sense

All the effects are assumed to be additive.

$$q_C q\ (1 + \varepsilon S + \varepsilon S + \varepsilon W)\ 2 \qquad \text{(Eq. 4)}$$

Following Lock's work, Mercker (see 2.1.2 (7)) evaluated the solid blockage for automotive testing, taking into account the slenderness of the model $\gamma = L/\sqrt{A}$ and the model volume V_M. The correction ε_S of Equation 4 may be expressed as:

$$\varepsilon_S = (1/2)\ \gamma\ \tau\ ((V)_M/V_T)\ 3/2 \qquad \text{(Eq. 5)}$$

where:

V_T = tunnel control volume (length of car · cross section of tunnel).

The test section boundary coefficient τ may be taken from Wüst (see 2.1.2 (4)). See, for example, Figures 2 and 4.

Concerning wake blockage effects, it has been thought for many years that this was negligible in open jet tunnels. It was thought that the jet expansion in the region of the model compensates exactly for the change of the effective speed past the model, but this is true only in a restricted sense. For car-like models creating a considerable wake, the corrections in open jet tunnels are moderately large and opposite in sign to those in closed tunnels. Following the example of Maskell (see 2.1.2 (8)) for closed tunnels, Sachs (see 2.1.2 (9)) suggested that it should be possible to express the wake blockage effects in open jets in the form of:

$$\varepsilon_W - K \cdot C_D \cdot (A/A_N) \qquad \text{(Eq. 6)}$$

where K is a blockage shape factor. The magnitude and character of the factor K can vary from tunnel to tunnel according to the precise details of layout and construction of the tunnel.

In order to evaluate the shape factor K, it is necessary to carry out some calibration measurements in the absence of any solid blockage interference. This can be achieved by measuring the drag coefficient of a series of square or rectangular flat plates of different size, normal to the flow. Flat plates have virtually no volume, giving $\varepsilon_S = 0$.

The horizontal buoyancy effect is due to a possible static pressure gradient along the axis of the test section. Considering a linear pressure gradient along the length of the model, the buoyancy force may be calculated:

$$\Delta C_{DB} = -\partial Cp/\partial L \cdot (VM/A) \qquad \text{(Eq. 7)}$$

So the entire blockage correction formula from Mercker and Sachs will have the form:

$$q_C = q\ [1 + (1/2)\ \tau\ \ \gamma(\ V_M/V_T)^{3/2} - KC_D(\ A/A_N)]2 \qquad \text{(Eq. 8)}$$

for the flow quantities, or

$$C_{DC} = C_D\ [\,1 + (1/2)\ \tau\ \gamma\ (V_M/V_T)\ 3/2\ - KC_D\ (A/A_N)\ - 2 + \Delta C_{DB} \qquad \text{(Eq. 9)}$$

for the drag coefficient.

A different approach has been discussed by Rogers (see 2.1.2 (10)), representing a wake by a source and simulating the boundary conditions by an array of images alternating in sign. The velocity increment associated with the wake blockage due to the presence of the images is zero, because the alternately positive and negative infinite sets of images produce zero velocity increment at the model position. The velocity gradient along the model length, however, is not zero.

Rogers shows that the incremental drag coefficient is the product of the measured drag and the solid blockage ε_S.

$$\Delta C_{DW} = C_D \cdot \varepsilon_S \qquad \text{(Eq. 10)}$$

Consequently, the above equation for q_C reduces to

$$q_C = q\,[1 + (1/2)\,\tau\,\gamma\,(V_M/V_T)^{3/2}]\,2 \qquad \text{(Eq. 11)}$$

for the correction of the stream quantities. The entire correction formula for blockage correction for the drag of a car-like model will then be

$$C_{CD} = C_D\,[1 + (1/2)\,\tau\,\gamma\,(V_M/V_T)\,3/2 - 2 \quad + \Delta C_{DB} + \Delta C_{DW} \qquad \text{(Eq. 12)}$$

In conclusion, the aforementioned theoretical or semitheoretical investigations, based on a very simplified mathematical model, show a large complexity of influence parameters.

Eccentricity of the model, lateral, and vertical extension of the model cross section, unsymmetrical model position and variation of the distances between nozzle exit and model and, as will be shown later, collector intake and the model, can have the same or an even larger influence than the blockage ratio (model-to-nozzle cross section ratio).

The theoretical investigations are all based on the principle of mirror imaging. Whereas, for a closed test section, the boundary condition is well defined, it may be questionable for an open jet test section where the free jet boundary consists of turbulent mixing zones varying in width and lateral velocity gradient with the jet path length.

4.2 Experiments—The correction formula of Maskell and Sachs (Equation 6) was verified for a special case by Owen (see 2.1.2 (11)) in the late seventies. In addition to the closed test section experiments, measurements were also performed in the Royal Aeronautical Establishment (RAE) 5 ft circular open jet tunnel (without ground plate). Owen used flat square plates for his experiments. The first intention was to use both force and pressure measurements. At an early stage of the measurements it was found that the drag and base pressure were markedly affected by the sting and balance used as support and to measure the drag. Only base pressures were used in the final measurements. The results of the six sharp edge plates are shown in Figure 8. The measurements led to the following approximation due to blockage, based on the method of Maskell:

$$\begin{aligned} C_D \cdot A/A_N < 3\% \qquad & \Delta q/q \sim -0.2 \cdot C_D \cdot A/A_N \\ C_D \cdot A/A_N < 3\% \qquad & \Delta q/q \sim -(C_D \cdot A/A_N)^2 \end{aligned} \qquad \text{(Eq. 13)}$$

The maximum geometrical blockage ratio in Owen's test was 6%.

In a test performed by Templin and Raimondo (see 2.1.2 (12)), rectangular flat plates were measured in three different test section configurations: solid walls, slotted walls with different open area ratio, and an open jet with ground plane. These plates had geometrical blockages up to 10.9%. The results are shown in Figure 9. Base pressures were also used as reference in these tests.

Whereas the closed wind tunnel results in Owen's and Templin's experiments agree quite well, the open wind tunnel results do not.

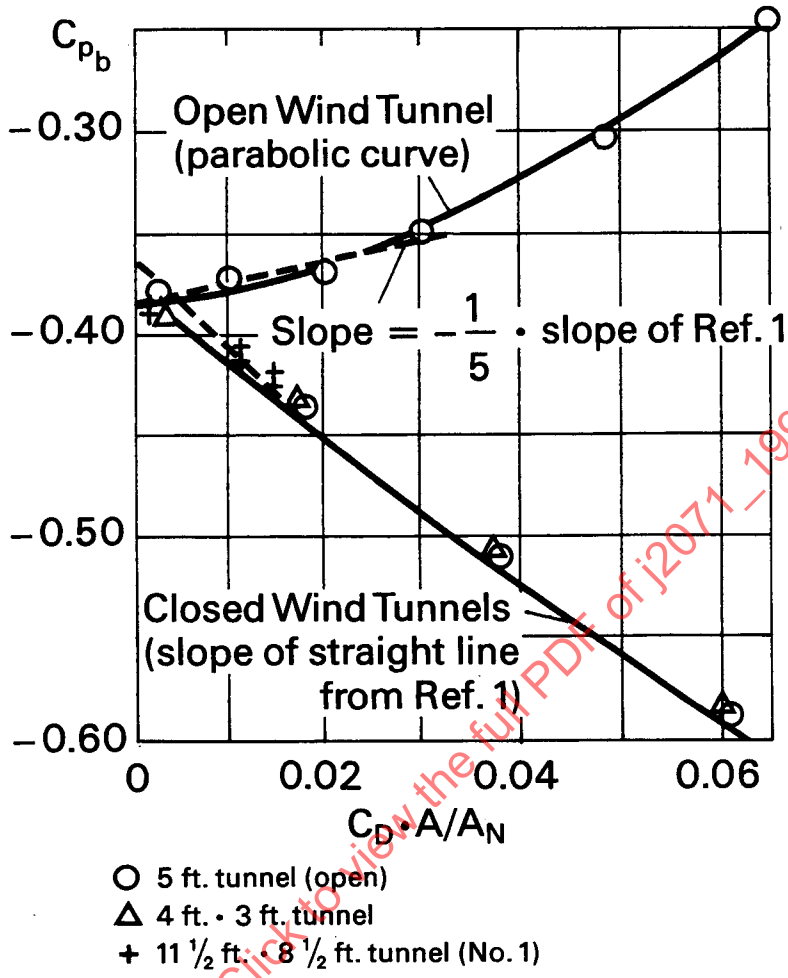

FIGURE 8—BLOCKAGE EFFECT ON BASE PRESSURE. NONLIFTING SQUARE PLATES AFTER REFERENCE 2.1.2 (11)

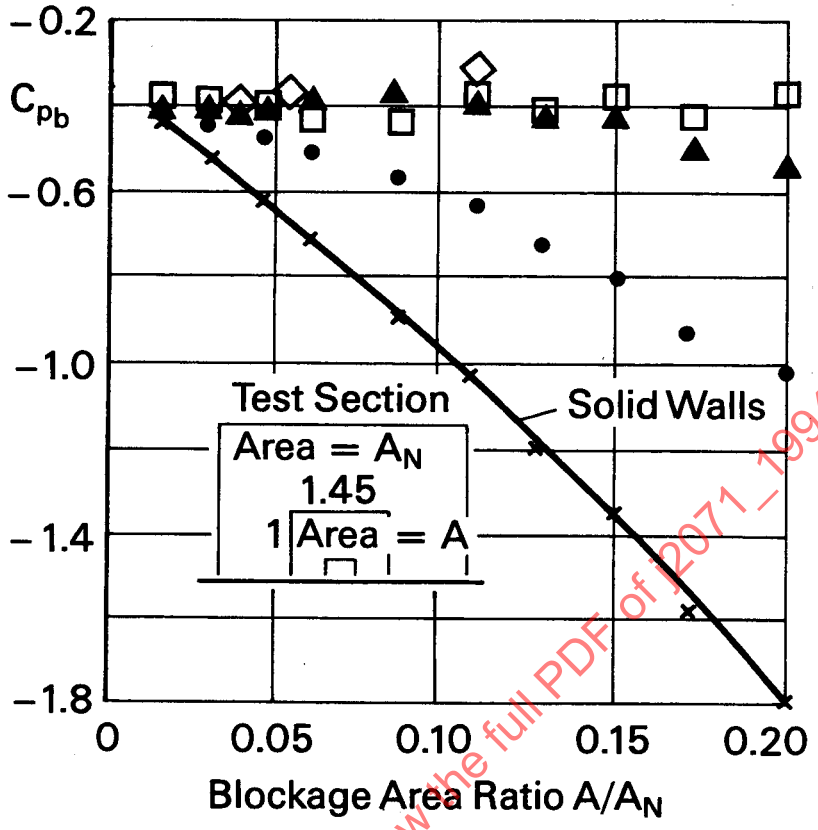

Symbol		Open Area Ratio of slotted Walls	Description
Measured	Predicted		
× ● △ ◇		0% 12% 30% 100% (⁄ Open Jet)	Measured in Pilot Wind Tunnels
	□	"Free Air"	Corrected solid wall using ovoid Interference velocities

FIGURE 9—BLOCKAGE EFFECT ON BASE PRESSURE.
NONLIFTING PLATES AFTER REFERENCE 2.1.2 (12)

From Templin's experiments in the open test section, a q-correction of about 3.5% can be derived at a blockage area ratio of 5.5%, whereas, from Owen's test, approximately 8% can be deduced at the same blockage area ratio. The lower values in Templin's test might be a consequence of the long test section used, which was relatively long in relation to the nozzle dimensions. Thus, there were no, or very little, collector influences.

For thin circular plates (see 2.1.2 (13)), drag measurements have been conducted for various plate sizes. In the experiments by Gerhardt and Kramer, the gap between plate and ground board was kept constant due to the drag measurement technique used. The relative gap height was h/D ~ 0.2 – 0.8.

The results of the measurements on circular plates show the trend to be expected from the theoretical considerations discussed before for solid and wake blockage (Figure 10).

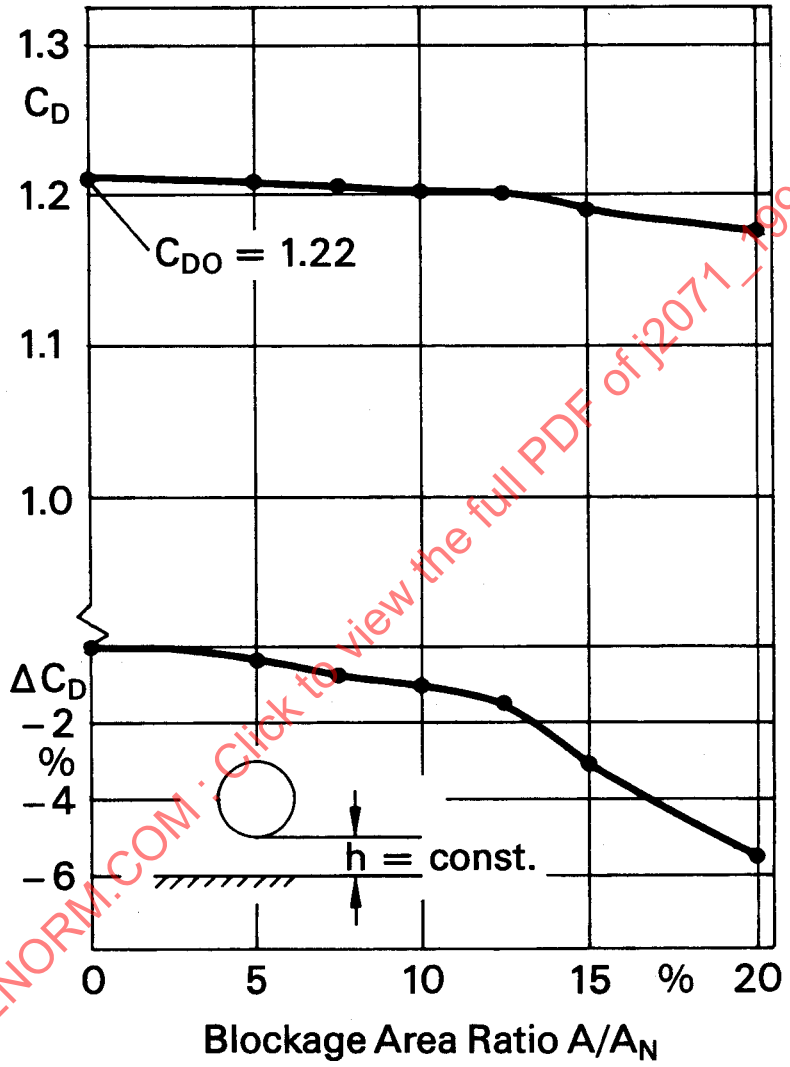

FIGURE 10—DRAG COEFFICIENT VERSUS BLOCKAGE
FOR THIN CIRCULAR PLATES AFTER REFERENCE 2.1.2 (13)

In the study by Mercker (see 2.1.2 (14)) a variety of model shapes were tested, including triangular, square and rectangular blocks with square plan view, and rectangular plates. Pressure measurements in the closed and open test sections were performed. The correction of the base pressure follows for open jet test sections by evaluating the cross-sectional area of the jet with and without a model at the model location:

$$C_{pbc} = C_{pb}/n + (n-1)/n \qquad \text{(Eq. 14)}$$

where:

n = $c \cdot (A_m/A_o)^2$
C_{pbc} = Corrected base pressure coefficient
C_{pb} = Measured base pressure coefficient
n = Correction factor
A_m = Free cross-sectional area of the jet with model installed
A_o = Cross-sectional area of the jet without model
c = Proportional factor (c = 1 for geometrical blockage < 25% in open jet)

In this experiment, A_m and A_o were defined by using the 95% intermittency factor of a turbulent shear layer with and without a model. The intermittency factor was measured with a hot wire probe.

In Figure 11 four different blockage ratios are corrected in an open jet experiment using the above formula. It is evident from the collapse of the open symbols that this method is quite effective.

In paper 2.1.1 (3) the correction formula of Wüst (see 2.1.2 (4)) for slender bodies, which is mentioned in 4.1, is compared with test results of rectangular boxes in the 37.5 m^2 climatic wind tunnel of VW. The results can be seen in Figure 12. The low gradient for the open tunnel, especially for low blockages, indicates that the error for not using a correction method might be small. However, for higher blockages, a compensating effect generated by the collector might occur because with increasing geometrical blockage, the longitudinal dimensions also increase and; therefore, the space between the rear end of the model and the collector intake area is decreased. This will be discussed later in more detail.

In a comparison paper by Cooper (see 2.1.2 (15)) , 1:10 scale trucks were tested in closed and open wind tunnels. The two trucks used in the tests were well detailed, each having both a high and a low drag configuration. For the open tunnel, the following correction was applied to the data:

$$C_D = (C_{Du} - 0.25\ \Delta C_{Db} \cdot \cos\Psi)\ (1 + 0.5\ A/A_2) \qquad \text{(Eq. 15)}$$

whereas the data of the closed tunnels were corrected by the formula:

$$C_D = (C_{Du} - \Delta C_{Db} \cdot \cos\Psi)\ (1 + -2\ A/A_2) \qquad \text{(Eq. 16)}$$

where:

C_D = Drag coefficient in body axis coordinates
C_{Du} = Uncorrected drag coefficient
ΔC_{Db} = Drag increment due to wake buoyancy
ψ = Yaw angle
A = Model frontal area
A_2 = Part of nozzle area above ground plane

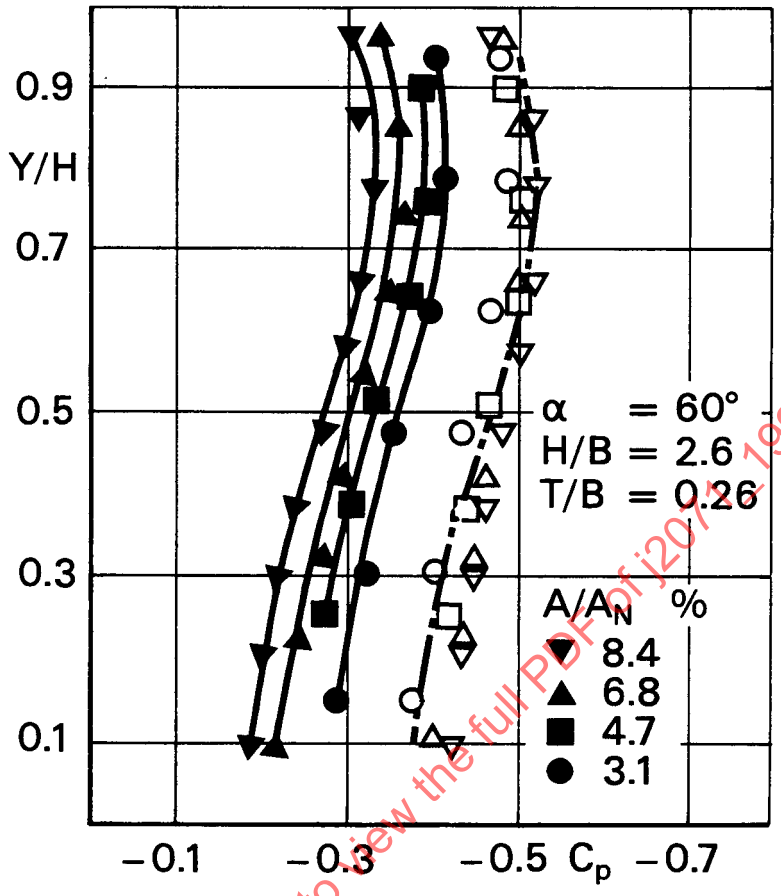

▼▲■● = C_{pw} measured
▽△□○ = C_{pwc} corrected
Y = coordinate along plate height
H = height of plate
B = width of plate
T = thickness of plate
α = angle of inclination of plate
A/A_N = blockage area ratio

FIGURE 11—CORRECTION OF WAKE PRESSURE OF A 60 DEGREE ANGLED PLATE IN AN OPEN JET TEST SECTION AFTER REFERENCE 2.1.2 (14)

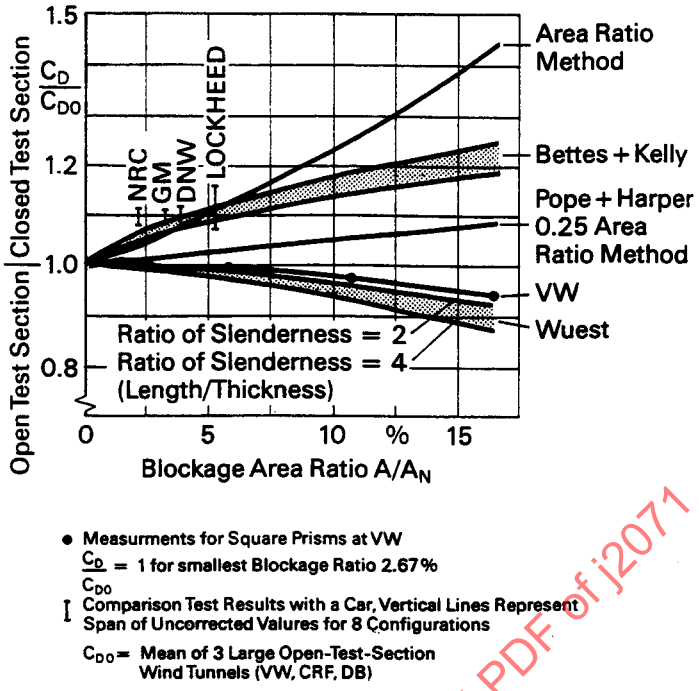

FIGURE 12—BLOCKAGE CORRECTION METHODS
VERSUS BLOCKAGE AREA RATIO AFTER REFERENCE 2.1.1 (3)

This correction was obtained from References 2.1.2 (11) and 2.1.2 (16). The results of the measurements with two models are shown in Figure 13. In almost all the configurations tested, the open jet showed the lowest values. Even when the values are adjusted for blockage and buoyancy, using the equations, the data spread reduces to only 15% of the mean values.

In experiments by Frimberger and Pucher (see 2.1.2 (17)) a set of sharp edged cubes was tested in eight open throat wind tunnels to investigate the influence of blockage. Only pressures in specific cross sections were measured. The main results were:

a. The front faces of the cubes were almost unaffected by blockage.
b. On all other faces the pressures measured were too low.
c. The tendency of pressure change with increasing blockage is different for each wind tunnel.
d. The tendency of pressure change with increasing blockage is different for each face of the cubes.
e. Correction factors for pressure and drag coefficients derived from the measurements are different (Figure 14).
f. The number of parameters, which varied in the wind tunnels, was too large to assign single influences to specified parameters.

The results of this section are discussed in Section 5.

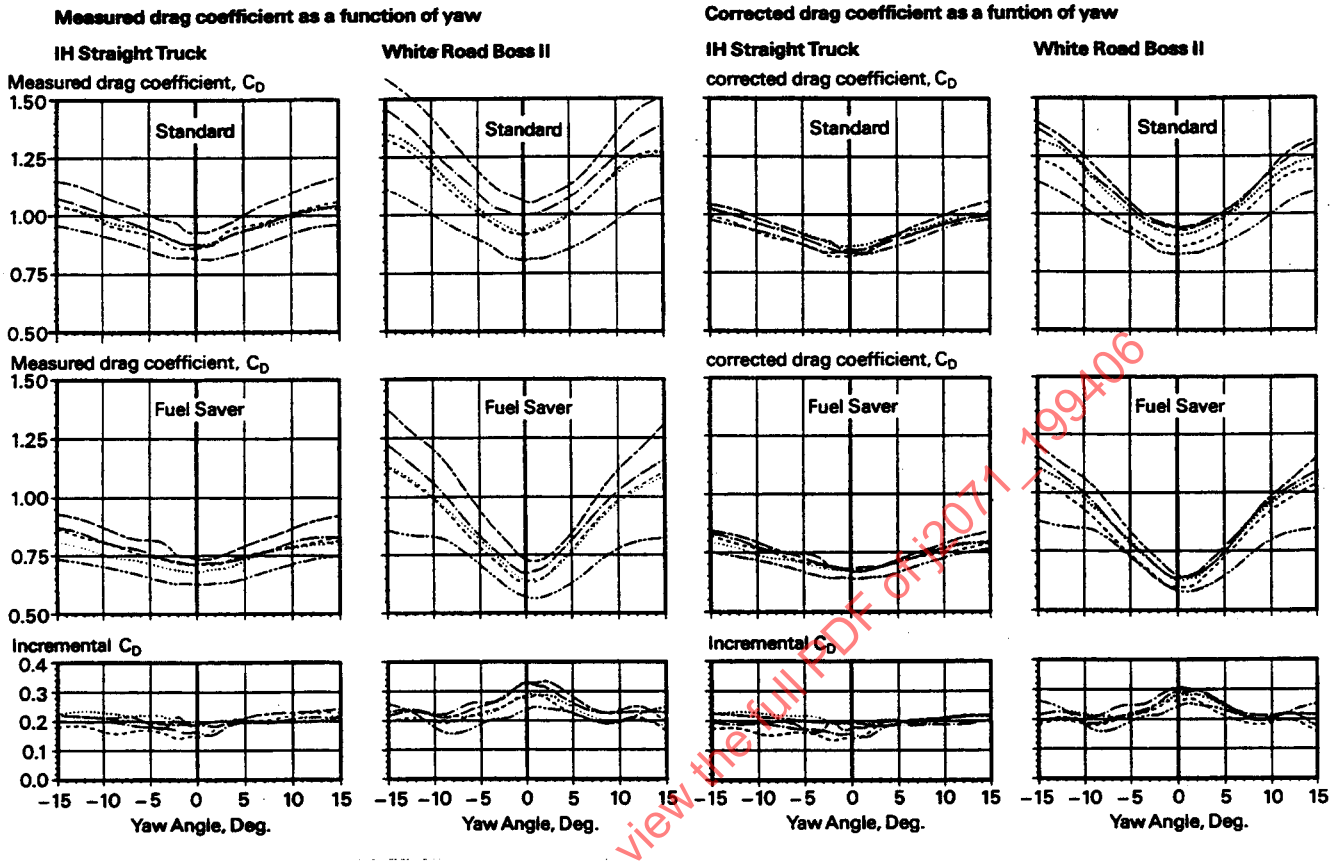

NRC = National Research Council of Canada
1,8 x 2,8 m^2 closed jet

NMI = National Maritime Institute, England
2,4 x 4,8 m^2 closed jet

LA = Fachhochschule Aachen, Germany
1,4 x 2 m^2 open jet

COA = College of Aeronautics, England
1,8 x 2,4 m^2 closed jet

MIRA = Motor Industry Research Association, England
1,0 x 2,1 m^2 closed jet

FIGURE 13—DRAG COEFFICIENTS OF 1:10 SCALE TRUCK MODELS IN DIFFERENT WIND TUNNELS AFTER REFERENCE 2.1.2 (15)

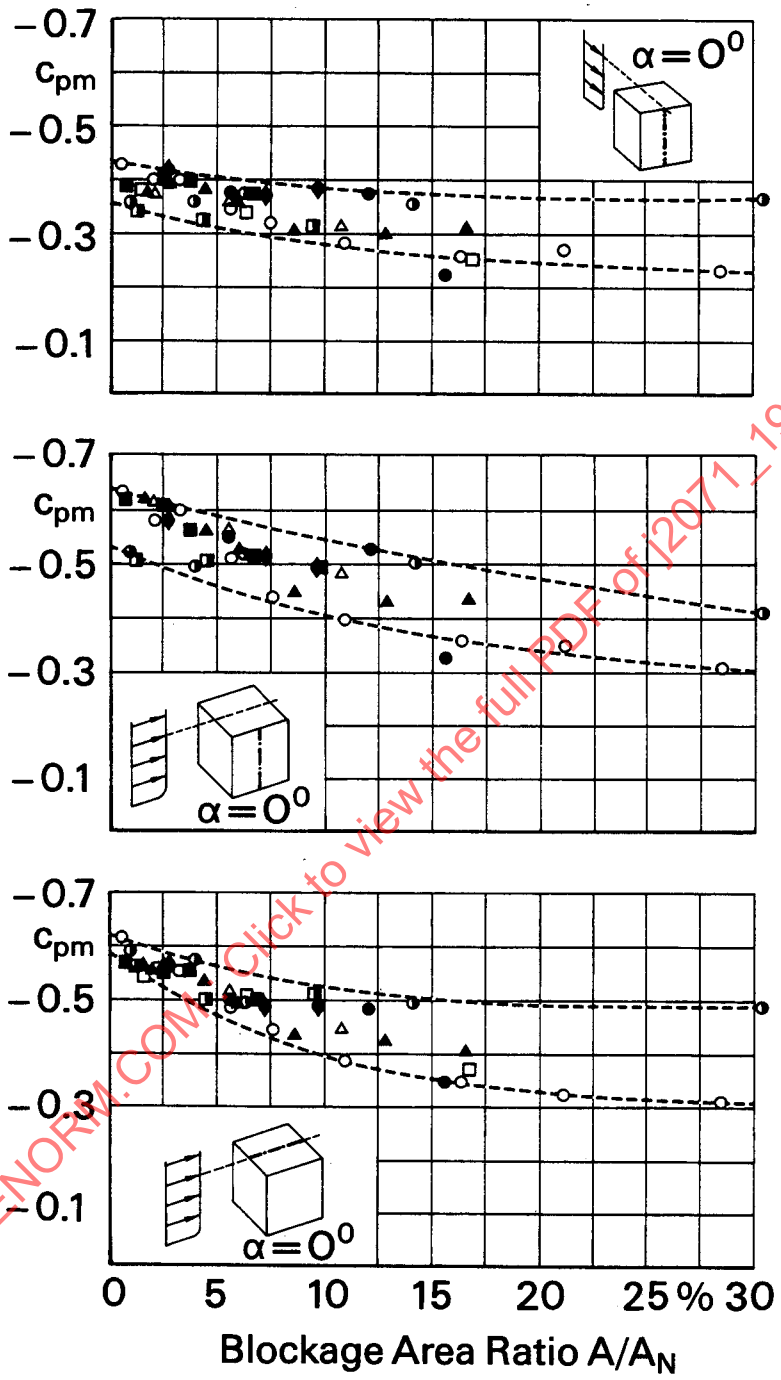

FIGURE 14—MEAN PRESSURE IN SPECIFIC LINES AS A FUNCTION OF BLOCKAGE IN DIFFERENT WIND TUNNELS AFTER REFERENCE 2.1.2 (17)

4.3 Influence of Test Section Design

4.3.1 GENERAL CONSIDERATIONS—The quality of an open jet test section is mainly determined by the sizing of the collector with respect to the test section dimensions. By turbulent exchange at the free boundaries of the jet discharged by the wind tunnel nozzle, turbulent mixing zones are established, the width of which increase with increasing jet path length. Consequently, the jet velocity profile in the mixing zones flattens with increasing length of the test section, and the portion of the jet cross section containing the volume flow discharged by the nozzle increases with increasing distance between nozzle and collector. The size of the collector should fit this cross section. Furthermore, the cross-sectional shape should be appropriate and it should be taken into account that the jet discharged by a rectangular nozzle becomes round due to turbulent diffusion and that this rounding effect increases with increasing jet path length. Therefore, for an open automotive wind tunnel, a collector with broken upper edges may fit better than a collector with a rectangular cross section. Of assistance in designing a collector may be a jet calculation described by Regenscheit (see 2.1.2 (18)) and Kramer et al. (see 2.1.2 (2)). In this simple calculation, the friction at the ground plate is not taken into account because the shear stresses applied to the jet, due to the turbulent mixing, are of a far higher order of magnitude. The collector cross section should be determined in such a way that the dividing streamline, separating the volume flow entering the collector from the volume flow recirculating in the plenum surrounding the test section, is in a stable position on the rounded leading edge of the collector. This procedure was described in detail by Kramer et al. (see 2.1.2 (19)).

The curvature of the leading edge of the collector is especially influential in the investigation of models under nonsymmetrical flow conditions. In this case, also, the position of the dividing streamline on the collector leading edge should be stable (Kramer and Gerhardt) (see 2.1.2 (20)).

For test sections that are short related to the nozzle dimension, the velocity profile in the mixing zone at the position of the collector still has a strong lateral gradient. Due to the steep gradient, a small misalignment of the collector position and/or the curvature of the collector leading edge can cause rather strong changes in the static pressure distribution along the test section. Therefore, a carefully designed collector is required. Because the entrainment flow for a short test section is relatively low, the volume flow recirculating in the plenum surrounding the open jet is relatively small. Therefore, for such a short test section, a relatively small plenum seems to be sufficient.

If full-scale cars have to be tested, a certain minimum length of the test section is required. Therefore, wind tunnels with smaller nozzle cross sections have a larger ratio of open jet length related to the nozzle dimensions. Also, the ratio of the entrained volume flow to the volume flow discharged by the nozzle is larger for those wind tunnels with relatively small nozzles. The open jet entrainment depends on the ratio of jet free circumference to the jet cross section, which is larger for a small nozzle than for a large one at the same open jet length. Therefore, for full-size wind tunnels with small nozzles, the mixing zone at the end of the test section, compared to the size of the test object, is much wider. This leads to a flatter total pressure gradient in the mixing zone at the collector distance. Consequently, the lateral variation of the dividing streamline, separting the flow into the collector from the recirculating flow, becomes less critical. From this it may be concluded that, for a large test section length in comparison to the nozzle dimension, a larger collector and a less sophisticated collector leading edge design may be appropriate. The recirculating volume flow, however, related to the volume flow discharged by the nozzle, increases noticeably. Therefore, such long test sections require much larger relative dimensions of the surrounding plenum.

4.3.2 EXPERIMENTS—V. Schulz-Hausmann and Vagt (see 2.1.2 (21)) performed experiments to evaluate the influence of the test section design. By varying the test section length by moving the collector upstream, the influence on the static pressure distribution in the longitudinal direction could be demonstrated. Figure 15 shows this correlation for a collector/nozzle ratio A_C/A_N = 1.96 with the test section length as parameter, which is given in dimensionless form L_T/D_N, where $D_N = 4\ A_N/(2B_N + 2H_N)$, the hydraulic diameter.

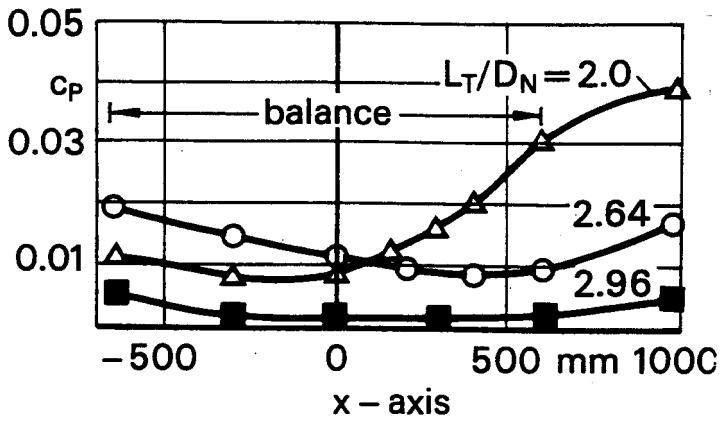

$A_C/A_N = 1.96$
A_C = collector area
A_N = nozzle area
L_T = test section length
D_N = hydraulic diameter of nozzle

FIGURE 15—STATIC PRESSURE DISTRIBUTION (EMPTY TEST SECTION) AFTER REFERENCE 2.1.2 (21)

In a second step, the collector/nozzle ratio A_C/A_N was varied. Figure 16 shows, among others, some test results for two identical models of different scale. Obviously, with a sufficient test section length, the results become independent of the nozzle collector ratio and the blockage ratio. In principle, for each test section length (more precisely, for each distance between rear end of model and collector), a nozzle/collector ratio can be defined where the test results are brought to an optimum ($C_D/C_{Dref} = 1$). But due to the high gradients of the slopes in the neighborhood of this optimum, a variety of results is easily introduced.

Furthermore, the results show a clear blockage dependency for small test section lengths and small nozzle collector ratios. This is probably due to the fact that the jet of an open test section expands differently with or without the model placed in the test section, creating different recirculation and entrainment flow in the surrounding plenum chamber.

Vagt (see 2.1.2 (22)) also measured the drag of four thin flat square plates in a full-size wind tunnel. During this test series, the blockage area ratio was varied (A/A_N = 4.48%, 5.43%, 7.01%, and 8.79%). Although the plate edges were rounded, no Reynolds number effect could be detected between velocities of 10 m/s and about 38 m/s. Figure 17 shows results for a fixed collector area. As the pressure gradient in that wind tunnel is practically zero and the wake formation for the three smaller plates is obviously independent of collector size, it is quite likely that the aproximation given by the solid line represents a blockage effect.

Some concern exists for C_{Do}, which was evaluated by linear extrapolation to zero area blockage. Therefore, in a strict sense, there is some uncertainty in the absolute value. This is represented by the upper and lower boundaries.

For the largest plate (A/A_N = 8.79%), the wake extends into the influencing region of the collector and, thus, the result is strongly dependent on the collector size. The effect of the collector, which is only present for the largest plate, is shown, as an example, by the vertical arrow.

Thus, in general, a possible combined blockage collector influence given by the broken line can be estimated.

Gerhardt and Kramer (see 2.1.2 (27)) carried out experiments with models resembling the Ford-Transit. Their experiments also show the influence of test section length and position of the model in the test section. The experiments were carried out in the Göttingen-type wind tunnel of the Fachhochschule Aachen. The ratio of model cross section to nozzle area, based on the nozzle area above the ground plate, was 3.3, 6.6, 13.2, and 26.4%. Figure 18 gives the most important wind tunnel and model dimensions and the relative position of the various models. The radii of the models were chosen to give a supercritical flow situation at maximum tunnel speed (V = 40 m/s), even for the smallest model. Figure 19 gives the static pressure variation with test section length 50 mm above the ground plate. In the area where the models are situated, the variation of the static pressure may be neglected. In Figure 20 the drag coefficient is plotted as a function of blockage ratio and yaw angle. Up to blockage ratios of approximately 13%, the decrease in drag, typical for automotive open test sections, is evident. The increase in drag for larger blockages is due to the contraction of the flow in the relatively narrow area between model and collector. This influence has been investigated using the larger models by varying the model position relative to the collector. With the largest model (A/A_N = 26.4%), the drag decreases from C_D = 0.266 to C_D = 0.264 and C_D = 0.256 if the distance between model rear end and collector increases from 236 mm to 296 mm and 476 mm.

With the smaller model (A/A= 13.2%) the drag decreases from C_D = 0.251 (distance = 476 mm) to C_D = 0.237 (distance = 518 mm) and to C_D = 0.220 (distance = 643 mm). This is due to the increase of the static pressure on the rear surface of the models.

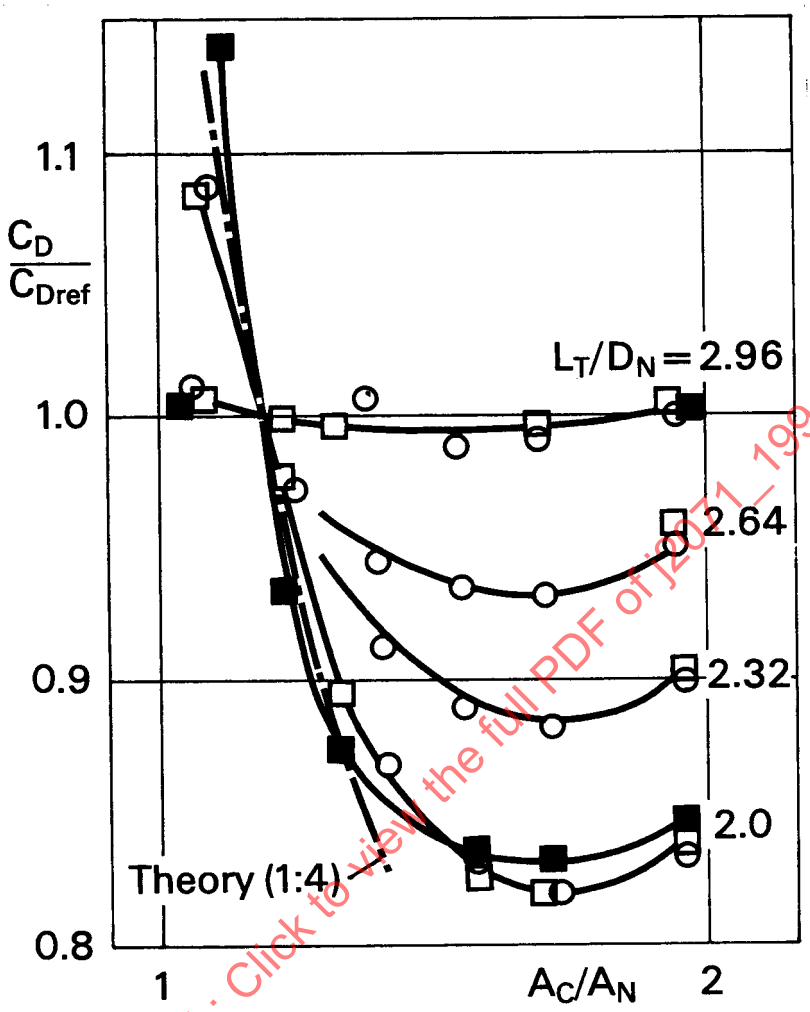

Model	scale	A /A_N [%]
Porsche 944	○ 1:4	8,3
MIRA Van	□ 1:4	8,3
	■ 1:5	5,3

A = model cross-section
A_C = collector area
A_N = nozzle area
L_T = test section length
D_N = hydraulic diameter of the nozzle

FIGURE 16—INFLUENCE OF RELATIVE TEST SECTION LENGTH AND RELATIVE COLLECTOR AREA ON DRAG COEFFICIENT AFTER REFERENCE 2.1.2 (21)

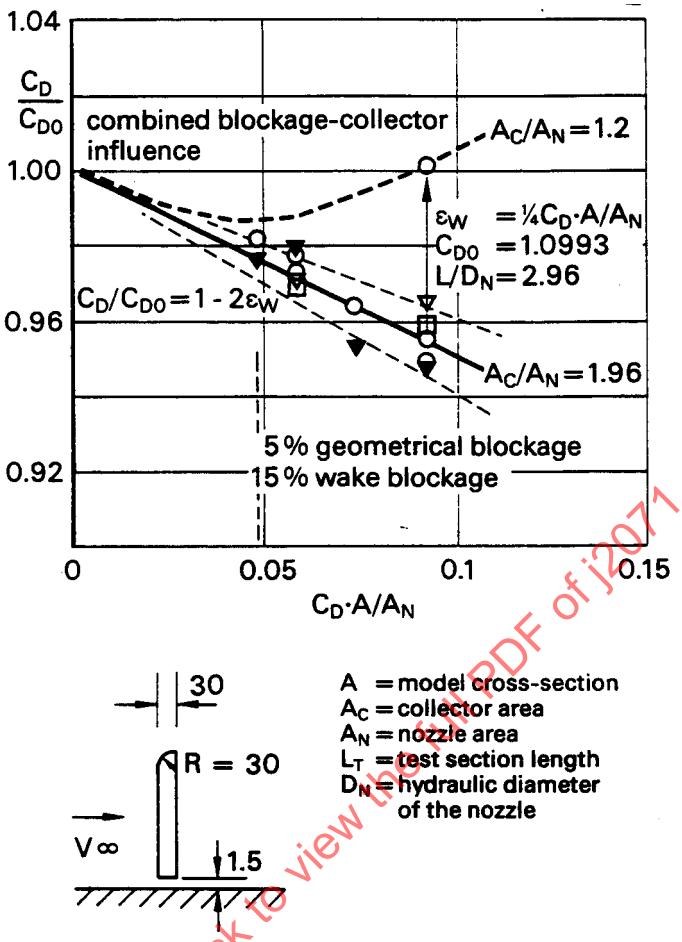

FIGURE 17—BLOCKAGE AND COLLECTOR EFFECTS
FLAT PLATE RESULTS AFTER REFERENCE 2.1.2 (12)

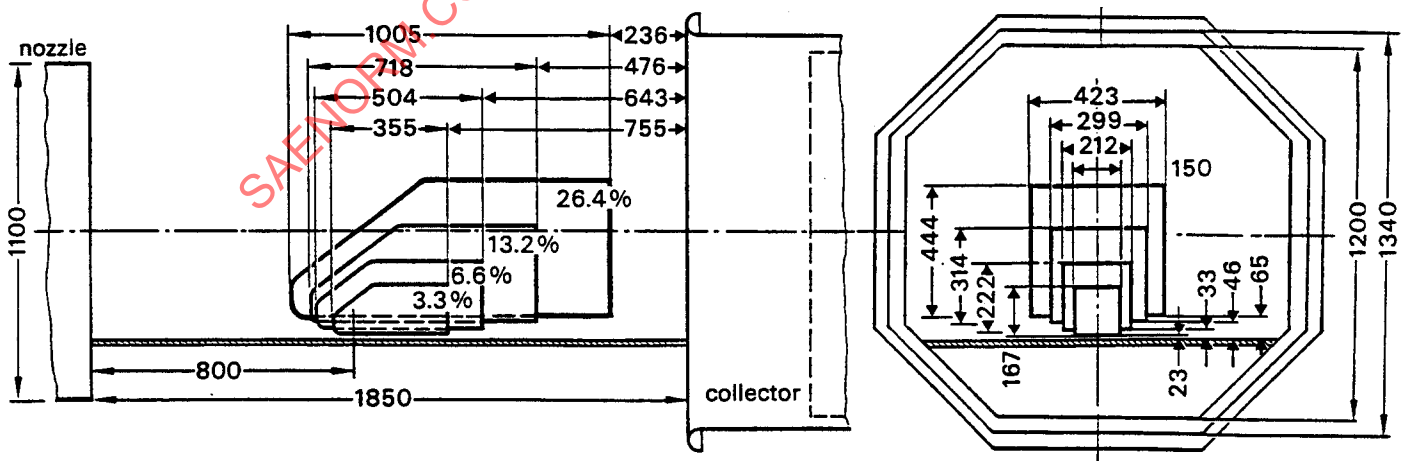

FIGURE 18—MODEL AND TEST SECTION DIMENSIONS AFTER REFERENCE 2.1.2 (13)

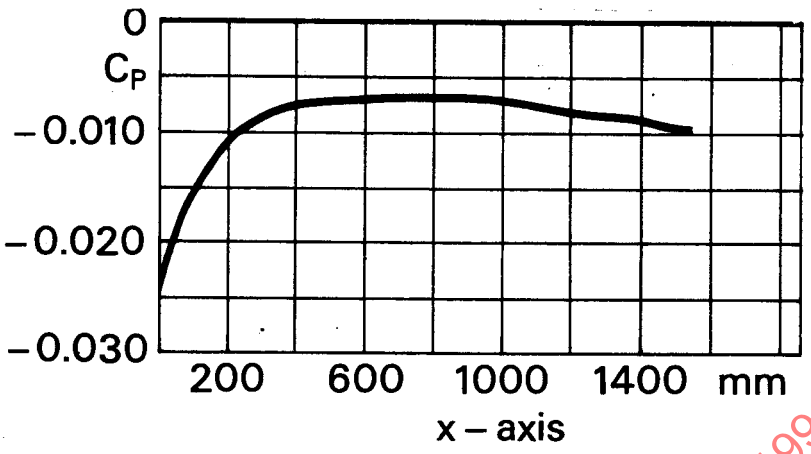

FIGURE 19—STATIC PRESSURE VARIATION IN FLOW DIRECTION FOR CENTER PLANE AT Z = 50 MM AFTER REFERENCE 2.1.2 (13)

4.4 Influence of Dynamic Pressure Measurement—Under certain conditions, the determination of the reference dynamic pressure or reference velocity can influence the aerodynamic coefficients especially at high blockage ratios.

The tunnel speed is usually defined as the mean flow velocity in the empty tunnel in that range of the test section that is occupied by the test object when the rate of mass flow is the same as for the case with the model present.

In general, this mass flow is measured in terms of static pressure differences between two sections of the tunnel of different cross-sectional area. Most commonly used are two sections within the nozzle. The first one is in the settling chamber and the second one at the nozzle exit (method 1: Δp-nozzle, Figure 21). Sometimes, the reference flow velocity is deduced from the difference between the static pressure in the settling chamber and the plenum (method 2: Δp-plenum, Figure 21).

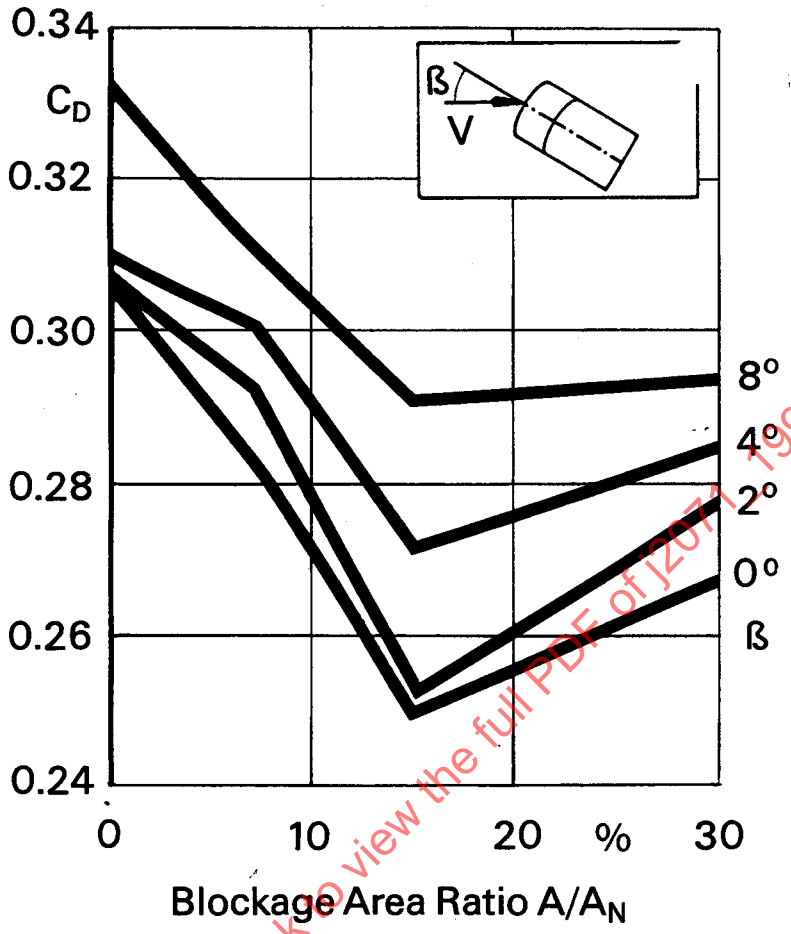

FIGURE 20—DRAG COEFFICIENT VERSUS BLOCKAGE AREA RATIO
AFTER REFERENCE 2.1.2 (13)

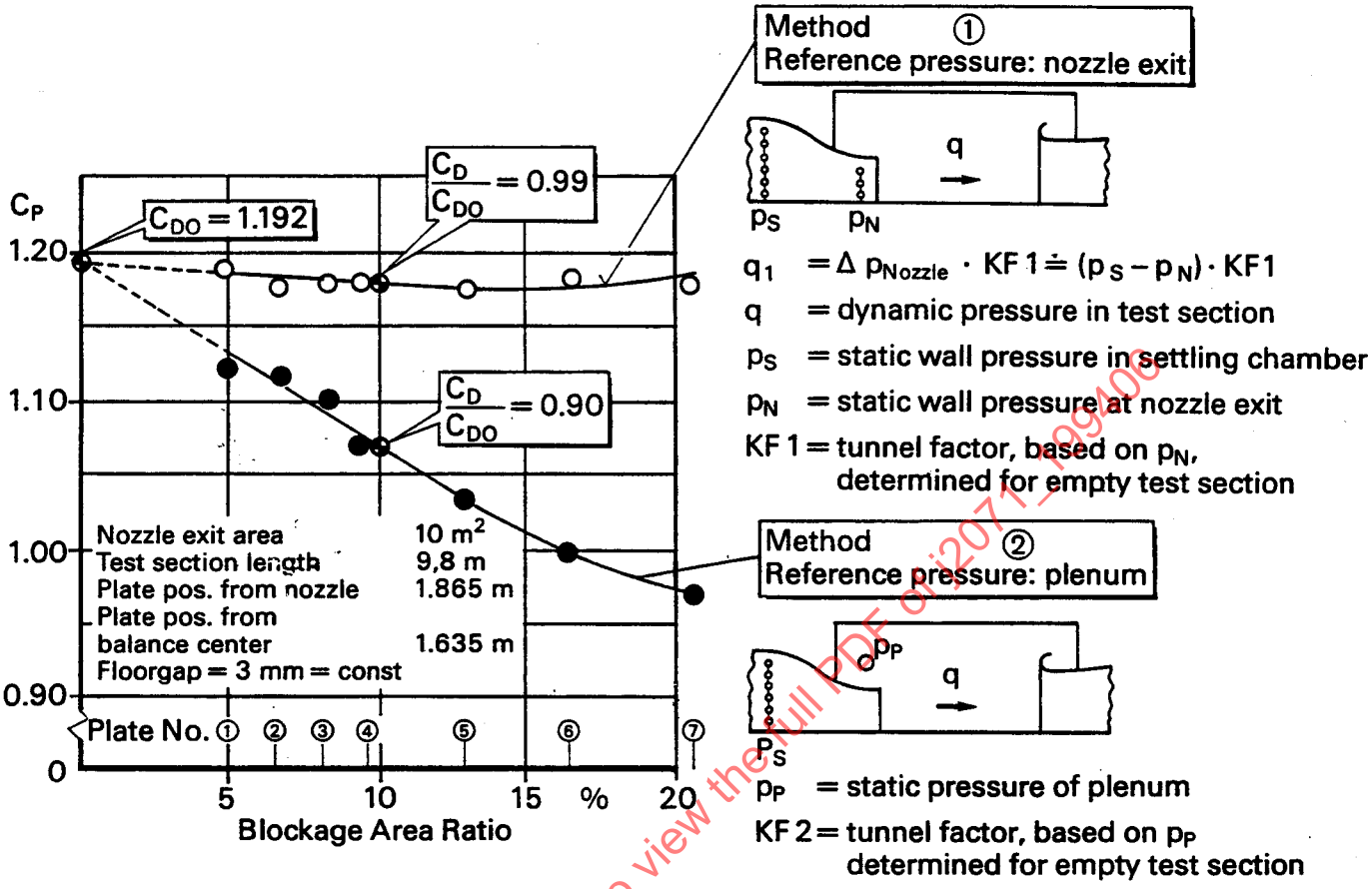

FIGURE 21—DRAG COEFFICIENT OF FLAT PLATES VERSUS BLOCKAGE AREA RATIO A/A_N FOR DIFFERENT METHODS OF DYNAMIC PRESSURE DETERMINATION; MEASUREMENTS FROM BMW ACOUSTIC WIND TUNNEL

For high blockage testing, the calculated aerodynamic coefficients using both calibration methods can be of completely different magnitude. In experiments with a luxury class car in the new BMW-Acoustic-Wind Tunnel (see 2.1.1 (8)) (blockage area ratio $A/A_N \sim 20\%$), the deviation in drag coefficients using the one or the other calibration method is around 7% ($\Delta C_D = 0.024$). Using flat plates (Figure 21) at 10% blockage ratio, method 2 (plenum pressure) yields a 10% drag reduction whereas method 1 (nozzle exit pressure) only gives a 1% drag reduction, related to zero blockage.

Detailed investigations about the determination of the tunnel speed using the plenum pressure in one case and nozzle exit pressure in the other case as reference are shown in 2.1.2 (23) and 2.1.1 (9).

Calibration method 1 (Δp-nozzle) uses information that is related to the flow or is proportional to the volume flow. Thus, the volume flow is kept constant for the empty test section and for the test section occupied by the car. This is simply done by increasing Δp-fan to maintain constant Δp-nozzle. The physical limit of method 1 is given by the requirement of an undisturbed velocity profile at the measuring position. Therefore, the pressure orifices have to be located significantly far away from the front of the test object, so that they are either not or only marginally influenced by the test objects presence. This requirement may cause problems in case of high blockage ratios. The most sensitive location is the exit plane at the end of the nozzle. Thus, to check the validity of the calibrations, the distributions of pressure coefficients have to be compared with and without the test object.

Calibration method 2 (Δp-plenum) uses the plenum pressure, which is determined by the surrounding condition (atmospheric). The plenum pressure is independent of the test object and, therefore, the same for the empty test section and for the test condition where the car is present. In case of high blockage ratios, the additional loss tends to raise the pressure difference Δp-plenum. If Δp-plenum is then kept constant, the volume flow will be reduced. The amount of reduction of volume flow is clearly dependent on the amount of the additional loss, which is determined by the size and the shape of the test object and its position within the test section. The drag coefficient, then, is calculated using the true force acting on the car and an apparent dynamic pressure that is too high. The resulting coefficient is too low. Thus, the determination of the reference velocity using the plenum pressure calibration procedure might be in error, if the calibration factor KF 2 remains unchanged for test conditions with high blockage.

4.5 Conclusions—The determination of drag data in automotive open wind tunnels is subject to various influence parameters, the classical blockage factor being only one of these. The effect of other wind tunnel specific parameters, such as collector size and shape with regard to the nozzle, collector distance from the model rear end, and model length with respect to the test section length, are also influential. The investigations performed on the subject to date are not conclusive with respect to detailed quantitative effects, but indications are that the effect of those parameters can be of the same, or higher, magnitude as the classical blockage factor. Therefore, correction of only the pure blockage effect will not be very helpful.

In order to support the conclusions and especially to get more reliable data, experiments precisely tailored to reveal the various influence parameters are required. The committee has started those experiments. Initial results will be presented in Section 5.

5. New Experimental Results

5.1 Unpublished Experiments by Committee Members:

a. Bluff Bodies: Data were made available both by Volkswagen AG and FKFS Stuttgart. Sharp edged rectangular boxes were tested in Volkswagen's climatic wind tunnel.

FKFS used eight sharp edged cubes. A fundamental advantage of wind tunnel investigations on bluff bodies is that their simple basic shape ensures geometric similarity of models. Moreover, the aerodynamic coefficients of bluff bodies are, in general, largely independent of Reynolds number. The disadvantage is that the aerodynamic behavior is not comparable with basic car shapes (ground clearance, detached flow in models, maximum cross-sectional area, wake). Drag coefficient C_D versus geometrical blockage ratio A/A_N for cubes and square boxes in unyawed condition is plotted in Figure 22.

b. Full-Scale Car and Van: In front of both Ford's full-scale nozzle (A_N = 23.75 m^2) and small nozzle (A_N = 8.64 m^2), a Citroen GS passenger car (different add-on parts, open and closed cooling) and a 1978 Ford Transit delivery van (open and closed cooling) were tested (Figure 23). Besides high blockage in front of the small nozzle, the question arises as to whether flow conditions (longitudinal static pressure gradient, flow angularity, uniformity of flow velocity, and boundary layer thickness) were the same in both wind tunnel variations. Due to both the add-on nozzle and collector, in the case of the small nozzle, the test section length was shortened from 10.5 to 6.1 m, yielding different influences of nozzle and, especially, collector on the vehicles. Figure 23 shows the drag coefficient versus geometrical blockage ratio of the different vehicle configurations. This results in two different mean gradients, but not, as would be assumed, separated into the bigger Ford Transit and into the smaller Citroen GS. The considerably higher gradient relates to the Citroen's configurations C and E. Both configurations have in common that the modifications influence the underbody flow of the car.

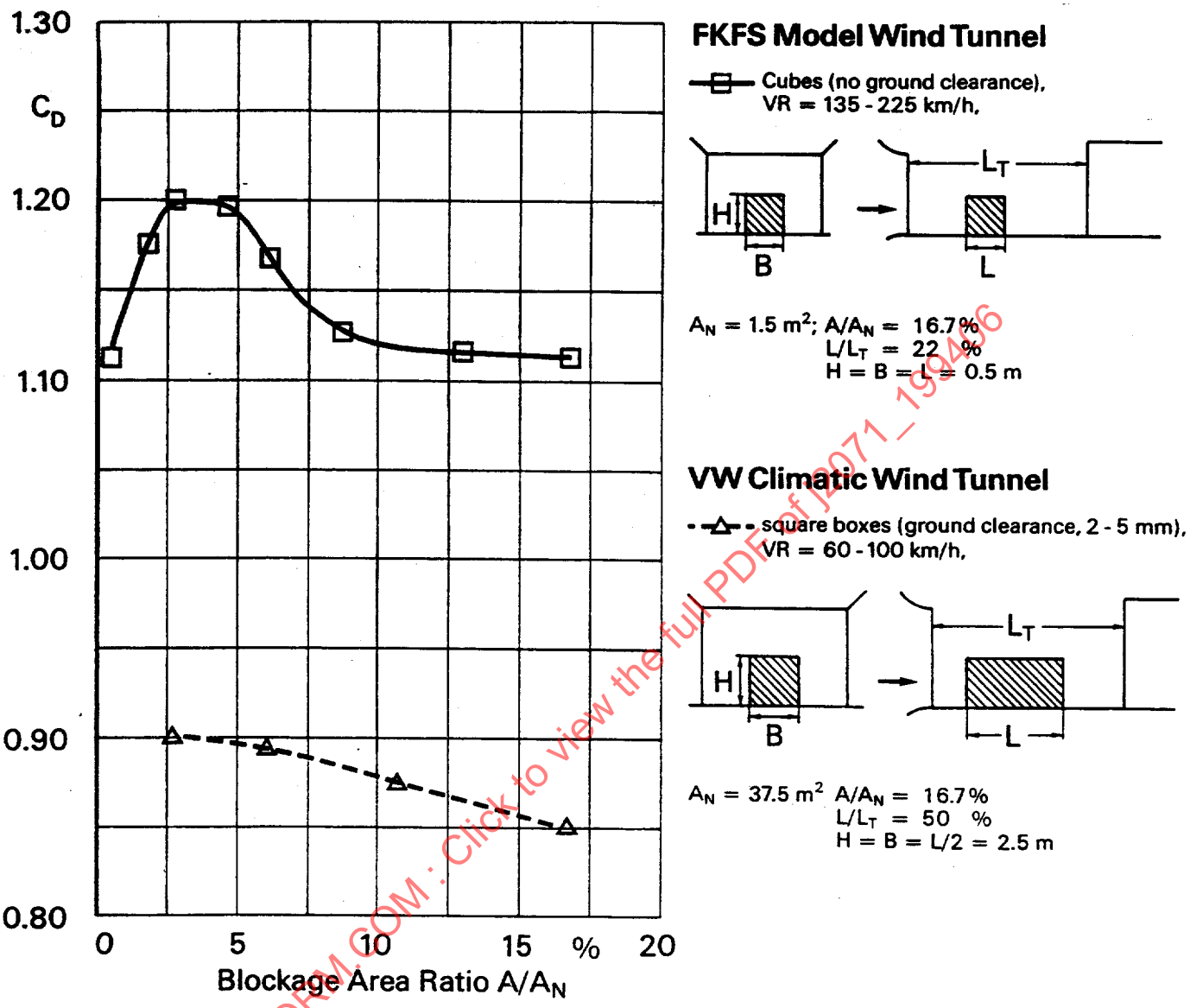

FIGURE 22—DRAG COEFFICIENT OF BLUFF BODIES AS A FUNCTION OF BLOCKAGE AREA RATIO

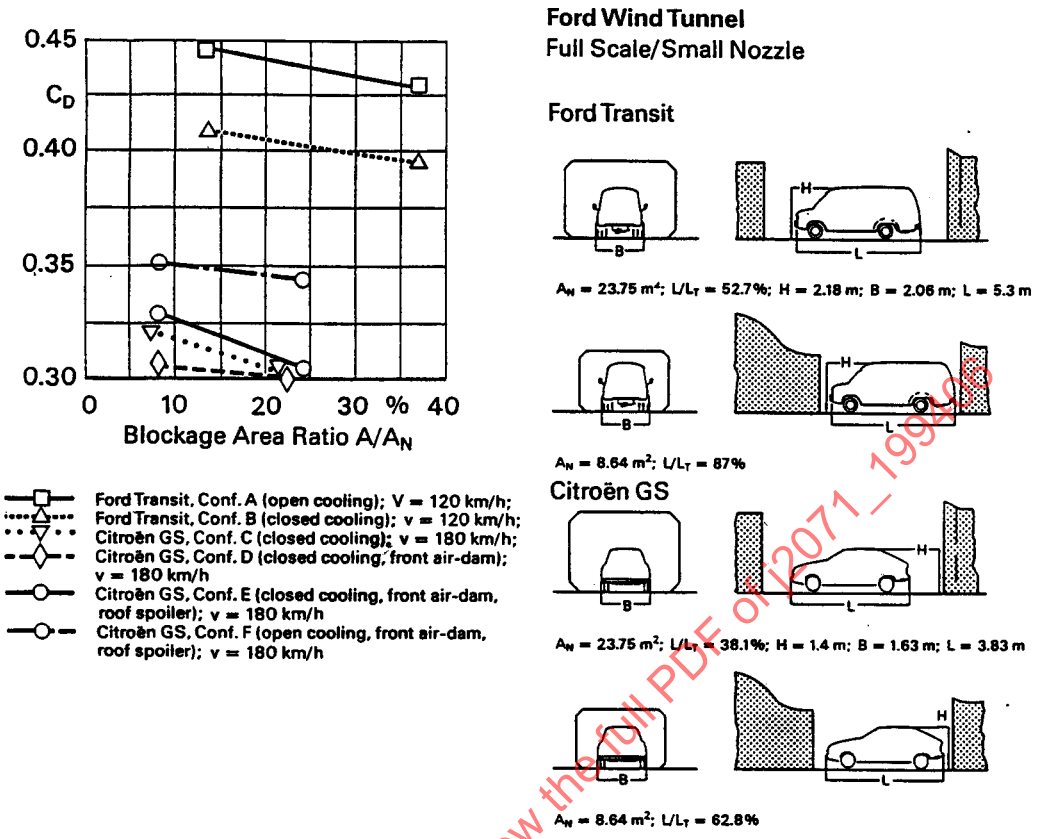

FIGURE 23—DRAG COEFFICIENT OF CARS AS A FUNCTION OF TEST SECTION LAYOUT

As can be seen from Figure 23, the high blockage ratio full-scale vehicles are very close to the nozzle and collector. Therefore, the nozzle and collector interference effects should be significant. Thus, the present cases represent more specific calibration factors rather than general wind tunnel blockage. In addition, the significant influence of test object and also, to some extent, of add-on parts can be seen from Figure 23.

5.2 Plates

5.2.1 RESULTS OF SQUARE PLATES WITH ROUNDED EDGES—In order to find a blockage correction method for car model testing in open test sections, it was proposed to use simple models, represented by thick square plates with three rounded edges for reference. The test arrangement at DLR is sketched in Figure 24. The dimensions of the square plate models are described in Table 4. Measurements with these plates were performed in the 8.6 m^2 DLR- and the 4.1 m^2 Volvo-wind tunnels.

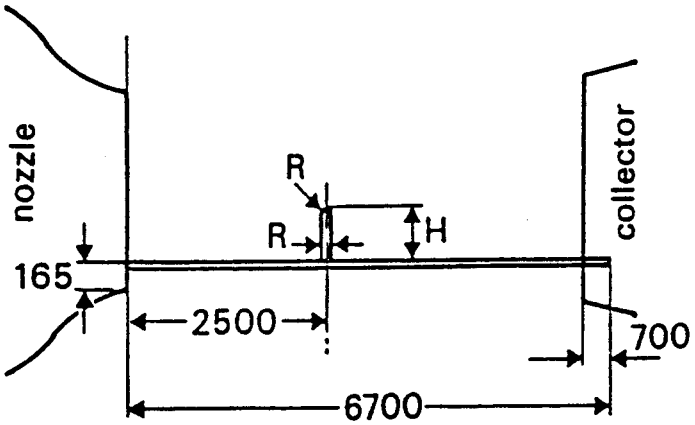

FIGURE 24—TEST ARRANGEMENT AT DLR

TABLE 4—SQUARE PLATE DIMENSIONS

Hardware for tests with thick square plates with rounded edges:

Thickness (mm)	Height (mm)	Radius (mm)	Frontal Area (m^2)	Blockage in DLR, Braunschweig (%)	Blockage in Volvo Wind Tunnel (%)
30.4	272	30.4	0.074	0.86	1.8
38	341	38	0.116	1.35	2.8
50.7	454	50.7	0.206	2.41	5.0
76	681	76	0.464	5.42	11.4
95	854	95	0.729	8.51	17.9
99.8	973	100	0.947	11.05	--
99.8	897	99.8	0.805	--	19.7

Radius and frontal area are chosen to correspond to those of the MIRA car models.
Therefore: height = frontal area
radius = height 8.96
thickness = radius

At DLR, six plate models have been manufactured (two out of aluminum and four out of wood). The wooden plates have rounded edges made out of a foam material with, compared to the aluminum edges, a relatively rough surface. The plate models were suspended on two cylinders that were fixed to a six component, strain gauge balance, Figure 25. The balance was located below the ground plate of the 3 m low speed wind tunnel of DLR Braunschweig, the test section dimensions of which are 2.8 m in height and 3.25 m in width (nozzle exit area). The ground plate itself extends from the nozzle exit to the collector inlet. Its surface is 165 mm above the lower nozzle wall, in order to remove the boundary layer. The ground clearance for all plate models during the tests was fixed at 4 mm. The distance from nozzle exit area to the plate model position on the ground plate was 2500 mm (Figure 24). The wind tunnel speed varied from 10 to 70 m/s, depending on plate size.

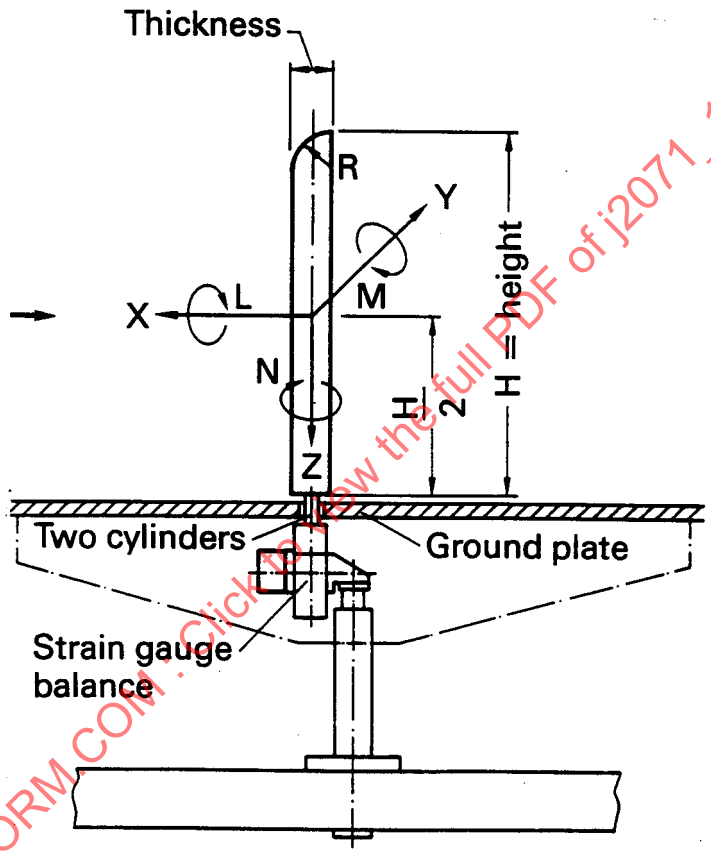

FIGURE 25—PLATE MODEL TEST ARRANGEMENT AT DLR

All the measurements have been taken with the plate models at the same position on the ground plate. It is, of course, obvious that this test arrangement includes one disadvantage, i.e., a varying parameter δ/H, where δ is the boundary layer thickness on the ground plate at model test position, and H stands for the plate's height. It was not possible to run the test with δ/H = const, because neither could the plate length in front of the model be varied nor could the plate model itself be shifted in the flow direction.

The boundary layer thickness at the model test position is about 35 mm (empty test section). The ratio varies, therefore, $0.13 > \delta/H > 0.04$. The influence of boundary layer is a reduction of the drag coefficient, the reduction being greatest for the smallest plate model.

A dependence of the drag coefficient C_D on the Reynolds number was noticed (Figure 26). The Reynolds number was calculated using the edge radius. The sharp decrease in drag at nearly the same Reynolds number for all plates is due to the flow around the plates' rounded edges where a critical Reynolds number, as in flow around cylinders, can be observed. The reason for the difference between the six plates may be explained by the different surface roughness of the rounded edges (see H. Schlichting, Grenzschicht-Theorie, page 614). The maximum speed of the wind tunnel (70 m/s) was not high enough to achieve the critical Reynolds number for the two smallest plates.

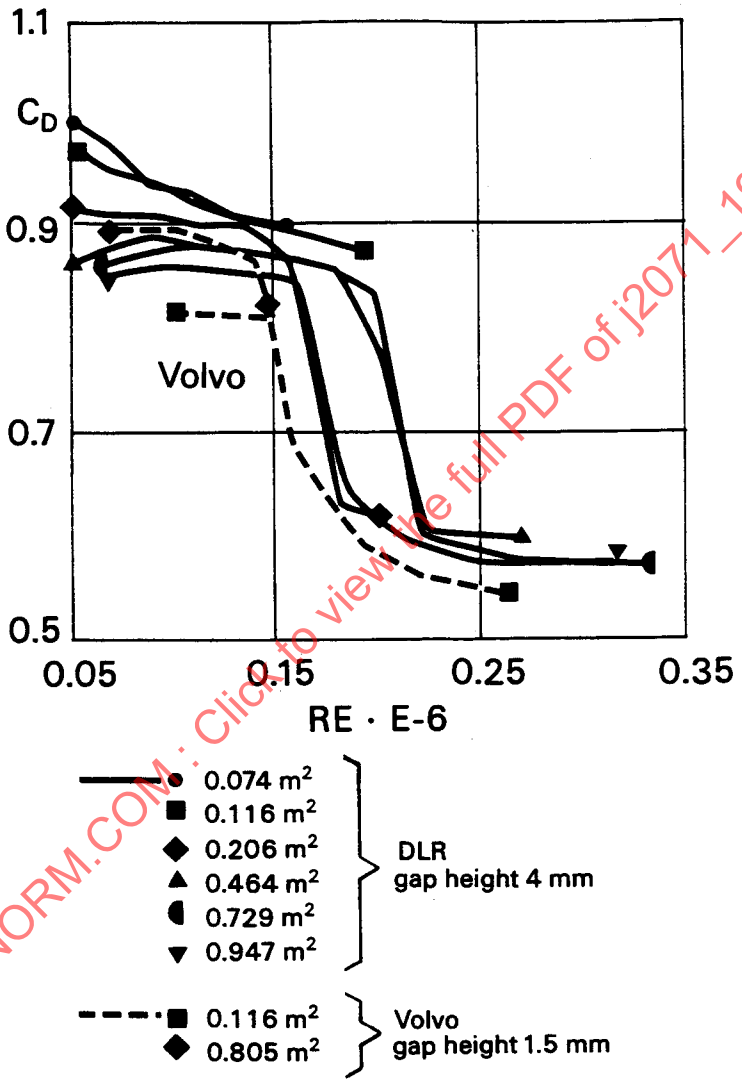

FIGURE 26—DRAG COEFFICIENTS OF PLATE MODELS WITH ROUNDED EDGES FACING THE FLOW

The largest plate model shows a slightly higher drag coefficient than the next smaller plate model. It is suspected that, due to the large wake region of this large plate model, the collector entrace pressure gradient exerts an influence.

Some results are compared with those measured by Volvo in Figure 26. The corresponding blockages are listed in Table 4. Volvo worked with a second set of similar plates with painted surfaces but with a different mounting. They did some preliminary tests with varying gap heights between floor and plates (Figure 27) and chose a gap height of 1.5 mm for the subsequent tests. Figure 28 shows the flow separation on the round edges for low and high Reynolds numbers in the Volvo wind tunnel. The difference in results between the DLR and Volvo tests is partly due to the difference in gap height.

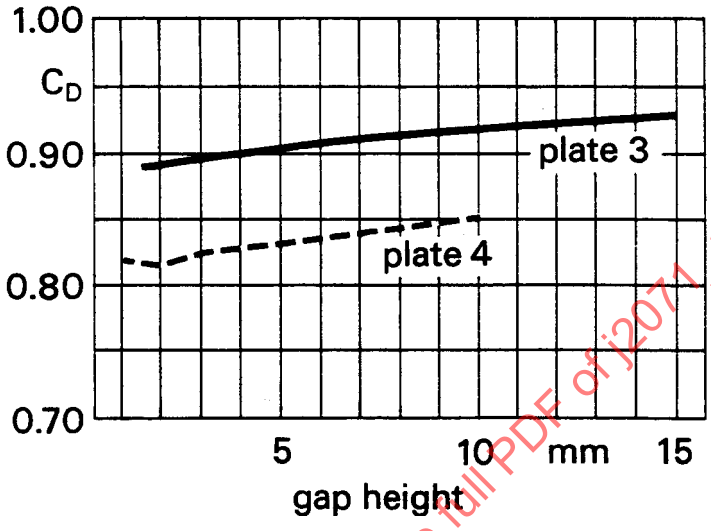

FIGURE 27—EFFECT OF FLAT PLATE DISTANCE FROM THE GROUND

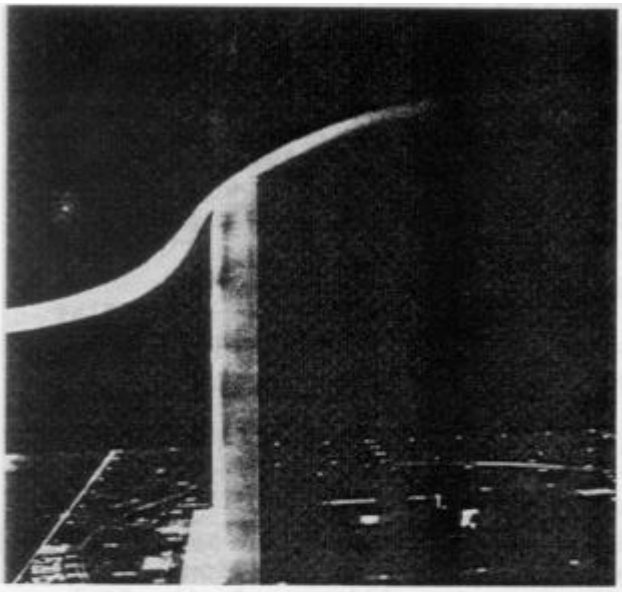

Photo 1
Square flat plate in VOLVO semi open test section
Low Reynolds number, separation on the round edge
Note the supporting struture

Photo 2
Square flat plate in VOLVO semi open test section
High Reynolds number,separation at the edge

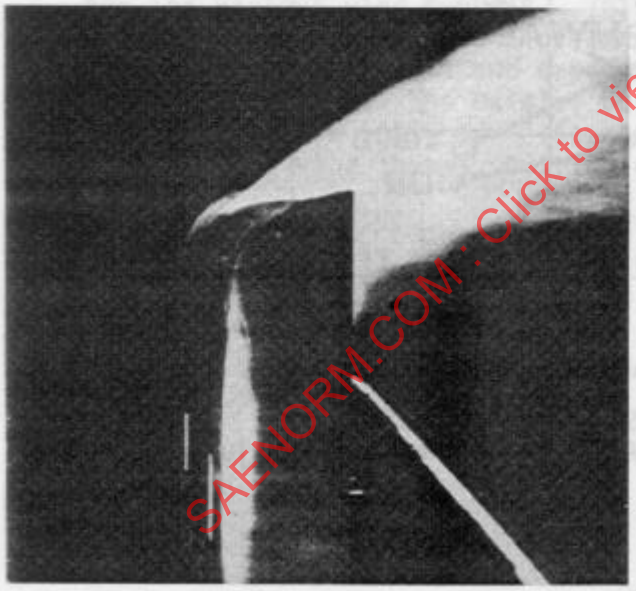

Photo 3
Flat plate with round edge at low Reynolds number
Separation at the middle of the radius

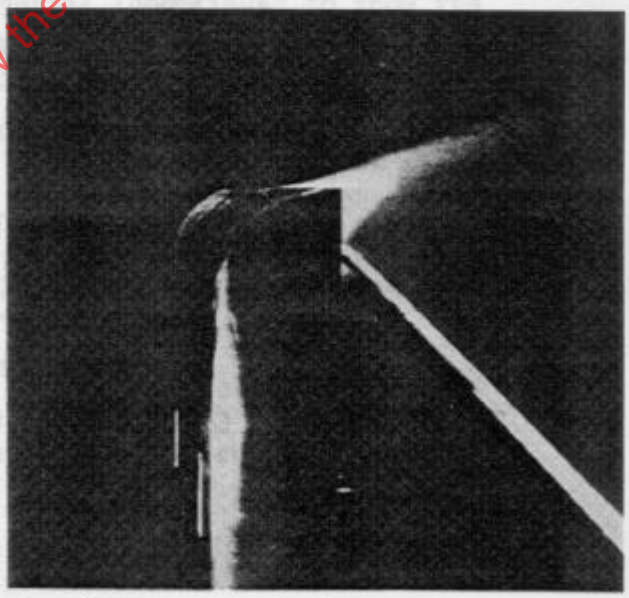

Photo 4
Flat plate with round edge at high Reynolds number
Separation at the edge

FIGURE 28—

Neither test series show a significant influence of size blockage with Reynolds numbers >$0.25 \cdot 10^6$, which correspond to radii of full-size cars. The data is not available in sufficient quantity to show a trend of drag change versus plate size (blockage) for supercritical Reynolds numbers. In particular, data on plates with small blockages and, therefore, valid information about drag at zero blockage (C_{DO}), is missing. Due to the attainable wind speeds, suitable tests cannot be done in the above mentioned wind tunnels.

5.2.2 RESULTS OF PLATES WITH SHARP EDGES—Measurements with sharp edged flat plates have been done by DLR (Braunschweig), Volvo, Daimler Benz, Fiat, Pininfarina, BMW aerodynamic wind tunnel, and BMW acoustic wind tunnel. DLR and Volvo used the same two plate sets described in 5.2.1, but with the sharp edges facing the flow. Daimler Benz used its own set of plates. Fiat and Pininfarina measured Pininfarina's set and BMW an additional set in both wind tunnels.

Figure 29 contains the results of the experiments. In addition, Figure 30 shows the results of Pininfarina, with changed positions. In the Fiat wind tunnel, the effect of changing the test position was small. The other experimenters did not vary the position.

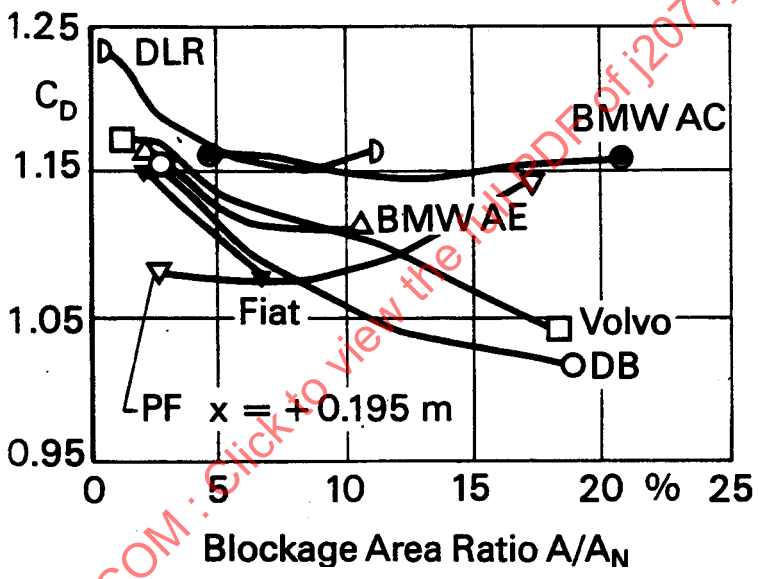

FIGURE 29—DRAG COEFFICIENTS OF SHARP EDGED FLAT PLATES VERSUS BLOCKAGE AREA RATIO IN DIFFERENT WIND TUNNELS

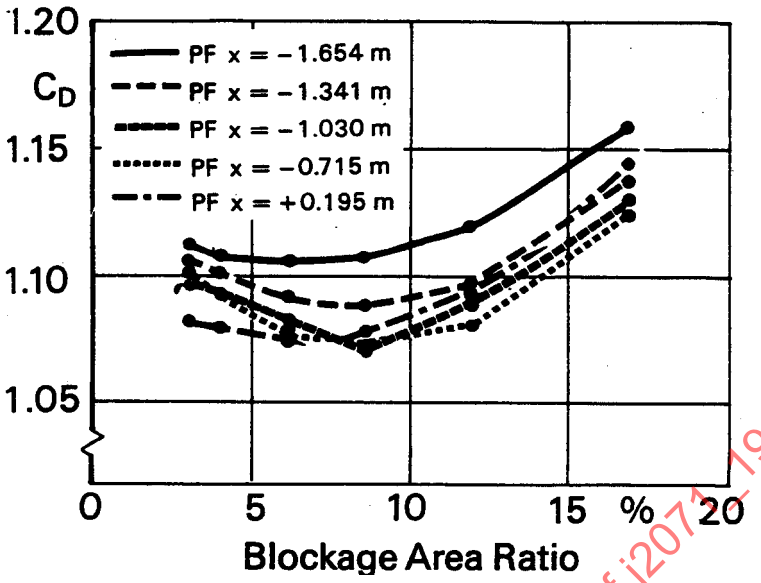

FIGURE 30—DRAG COEFFICIENTS OF SHARP EDGED FLAT PLATES IN PININFARINA WIND TUNNEL AT DIFFERENT POSITIONS (X = DISTANCE FROM BALANCE CENTER)

Figure 31 contains the same result as Figure 29, but with normalized drag. It is difficult to determine exactly the basic value of drag with zero blockage (C_{DO}) from Figure 29. In this case, the C_{DO} values have been chosen to achieve the best fit of the curves at $C_D \times A/A_N = 3\%$ and with respect to the trend of the curves in Figure 29. From Figure 31 can be derived a certain order of the blockage dependent normalized drag for the various wind tunnels. This series is believed to show the beginning of the collector influence but does not correspond to any influence of other site and experimental parameters for the same wind tunnels (Table 5). The Daimler Benz wind tunnel, for example, has a smaller relative collector area and a smaller relative test section length than Volvo's wind tunnel, but the collector influence starts at a larger blockage.

For this reason, it is not sufficient to look only at overall dimensions to describe tunnel behavior. Details such as collector shape are considered to be important also.

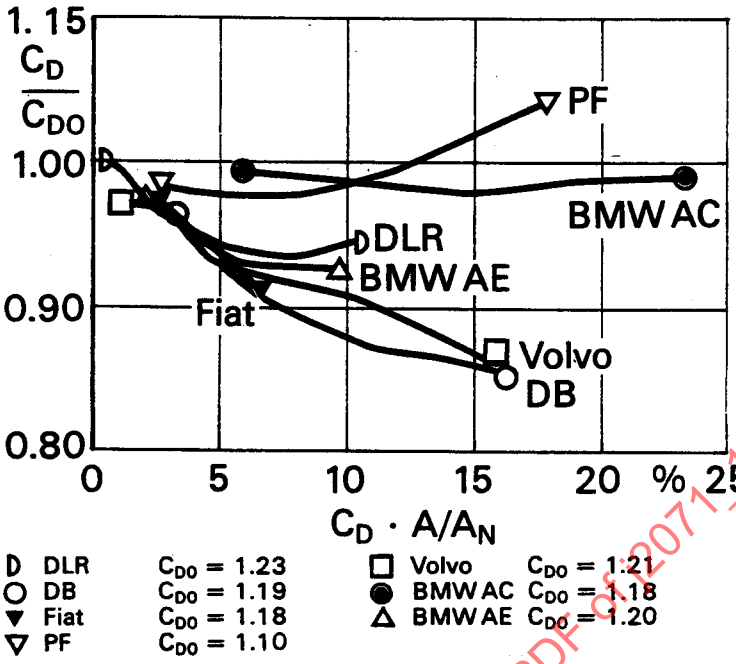

FIGURE 31—RELATIVE DRAG COEFFICIENTS OF SHARP EDGED FLAT PLATES

TABLE 5—FLAT PLATE MOUNTING DETAILS

	gap height (mm)	A_C/A_N	L_T/D_N	X/L_T	LT-X H (5%)
DLR	4	1.19	1.81	0.43	5.2
Volvo	1.5	2.97	3.85	0.283	13.9
DB	2.5	1.4	1.94	0.500	3.9
FIAT	0	1.35	1.70	0.407	5.1
Pininfarina	0	1.47	2.07	0.484	5.4
BMW AE	2	1.11	2.31	0.307	6.9
BMW AC	2	2.26	3.09	0.183	11.4

A_C = collector area
A_N = nozzle area
L_T = test section length
D_N = hydraulic diameter of nozzle
X/L_T = model reference point
H (5%) = height of square plate with a blockage of 5%

5.3 Results of Tests With Simplified Car Models—In order to find a blockage correction method for car model testing in open test sections, it was proposed to investigate simplified car models in different wind tunnels. The models were designed and supplied by MIRA (MIRA Models). Details and the theoretical dimensions of the models are given in Table 6 and Figure 32. By changing the rear part of each model, a notchback, a fastback, and a station wagon model could be produced.

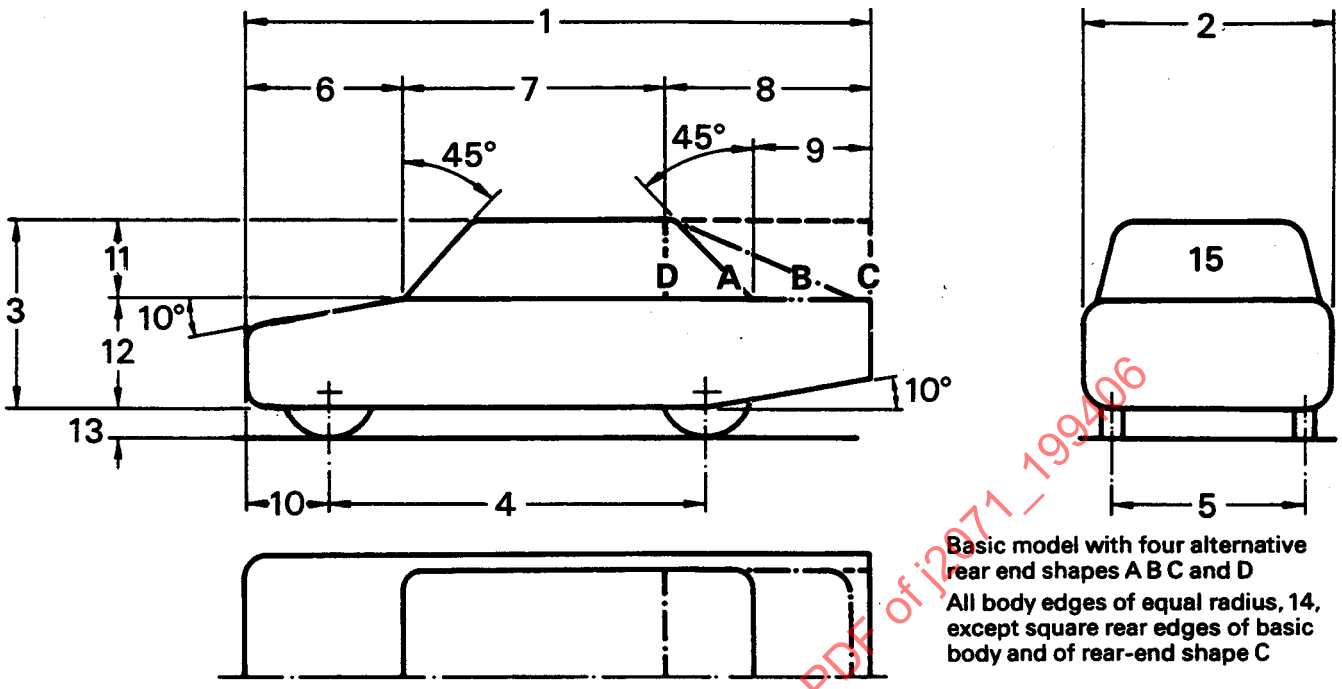

FIGURE 32—DIMENSIONS OF MODELS USED FOR BLOCKAGE STUDY (SEE ALSO TABLE 6)

TABLE 6—PRINCIPAL DIMENSIONS OF MIRA REFERENCE MODELS (SEE ALSO FIGURE 32)

	Model Scale	1:5	1:4	1:3	1:2	1:2	1:1	1:0.8
1	Overall length	833	1041	1389	2082	2945	4165	5206
2	Overall width	325	407	542	812	1149	1625	2031
3	Overall height	284	356	474	710	1005	1420	1775
4	Wheelbase	508	635	847	1270	1796	2540	3175
5	Track, front and rear	254	318	423	635	898	1270	1588
6	Bonnet length	211	264	351	527	746	1055	1319
7	Front canopy length	358	447	597	895	1266	1790	2238
8	Rear end length	264	330	440	660	933	1320	1650
9	Boot length (notchback)	150	187	250	375	530	750	938
10	Front overhang	107	134	178	267	378	535	669
11	Canopy height	102	127	169	254	359	508	635
12	Lower body height	142	177	237	354	501	708	885
13	Ground clearance	41	51	68	102	145	205	256
14	Radius of rounded edges	30	38	51	76	107	152	190
15	Frontal area, m^2	0.074	0.116	0.206	0.464	0.928	1.856	2.900

All dimensions in mm except where stated otherwise.

Results are available from BMW, Daimler Benz, DLR, FHS Aachen, FIAT, FKFS, Ford, IVK, Pininfarina, and Porsche. The overall test conditions for the MIRA Van in some model wind tunnels are shown in Figure 33. The edges drawn on the van model represent the "trailing edges" of the 1:5 and 1:4 models. It can be seen that the location of the model and the distance of the front and the rear from the nozzle and from the collector are quite different in the various test sections.

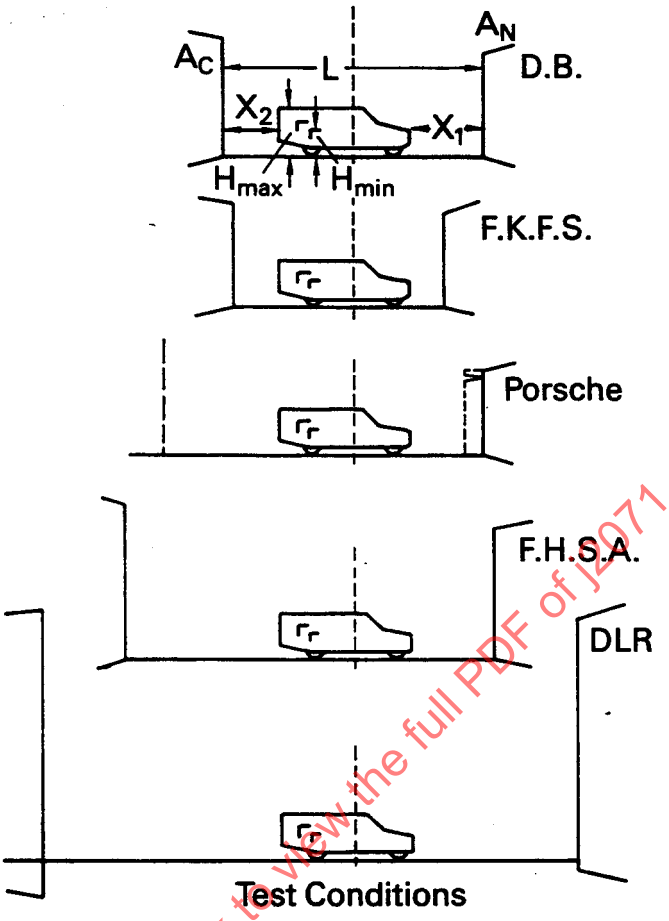

FIGURE 33—TEST CONDITIONS IN MODEL WIND TUNNELS
OF DAIMLER BENZ, FKFS, PORSCHE, FACHHOCHSCHULE AACHEN, DLR

In Table 7 some relevant wind tunnel specifications, test section dimensions, and model mounting details are given.

TABLE 7—WIND TUNNEL SPECIFICATIONS TEST SECTION DIMENSIONS MOUNTING DETAILS

	Aachen	DB	FKFS	Porsche	DLR
Test section	open	open	open	open	open
L_T/D_N	2.53	2.28	1.89	2.96	2.06
A_C/A_N	1.56	1.44	1.37	1.95	1.19
$X_1/(H_{max})$	1.8	1.6	0.76	1.6	3.5
$X_2/(H_{max})$	3.36	1.2	1.0	2.4	5.0
$X_2/(h_{min})$	7.14	3.2	3.0	5.4	9.3
pressure level variation ΔCp		<0.03	<0.008	<0.01	
Flow uniformity (typical)		±1%	±0.6%	±0.2%	
gap between wheel and TS-floor		1 mm	0.8-4 mm according to ground clearance specification	about 4 mm according to ground clearance specification	about 4 mm according to ground clearance specification
test speed	100 km/h	90–200 km/h	173–195 km/h	90–200 km/h	36–250 km/h
geometr. blockage	2.75%; 4.31% 7.66%	4.6%; 7.3%; 12.9%	4.9%; 7.7%; 13.8%	5.3%; 8.3%; 14.7%	0.9%; 1.3%; 2.4%; 5.4%; 10.8%

General Remarks About the Models:

a. The wheel mounting planes of the models were not flat. Because in some cases there was no provision for fastening the models, different model attitudes under different aerodynamic loads were found. the difference in drag was about 2%.

b. Different model heights were used during the test program. In some cases, shims of 4 mm thickness between wheels and test section floor were used to adjust the ground clearance to the values given in the specification. This has some influence on the absolute values, as shown in Figure 34.

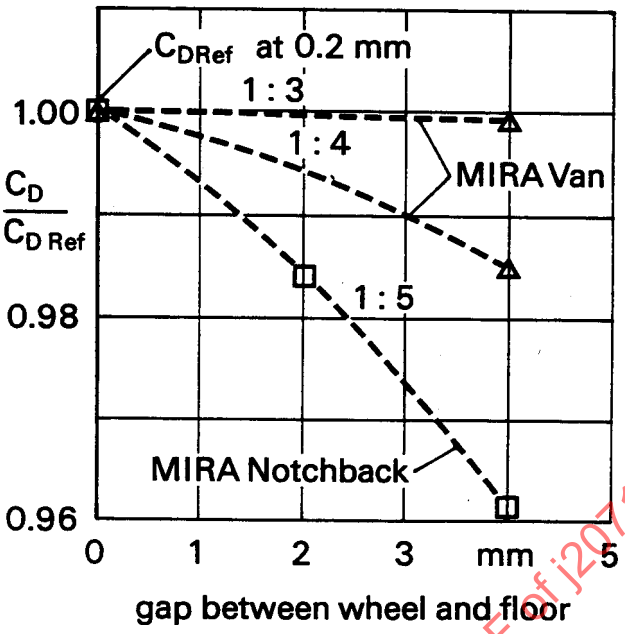

FIGURE 34—GAP INFLUENCE MEASURED IN PORSCHE WIND TUNNEL

c. In some cases, experimenters observed that the add-on parts of the models lifted a little at high wind speeds. It is possible that such effects have not been detected in all cases and, therefore, some results are in error.

d. Measurements show that the real frontal areas of the models differ up to 2.5% from the theoretical values of Table 6. Exact comparisons reveal that the differences are not only caused by wrong scaling factors but partly by geometrical dissimilarities. The C_D values discussed here are computed with the real measured frontal areas.

A comparison of the data measured in different wind tunnels (Figures 35 to 37) shows that the small MIRA models were measured in velocity ranges, which DLR and Porsche have shown to be very sensitive to Reynolds number. These Reynolds number effects are superimposed on the influence of the wind tunnels and the models. It is difficult to isolate a clear blockage effect reliably from these figures.

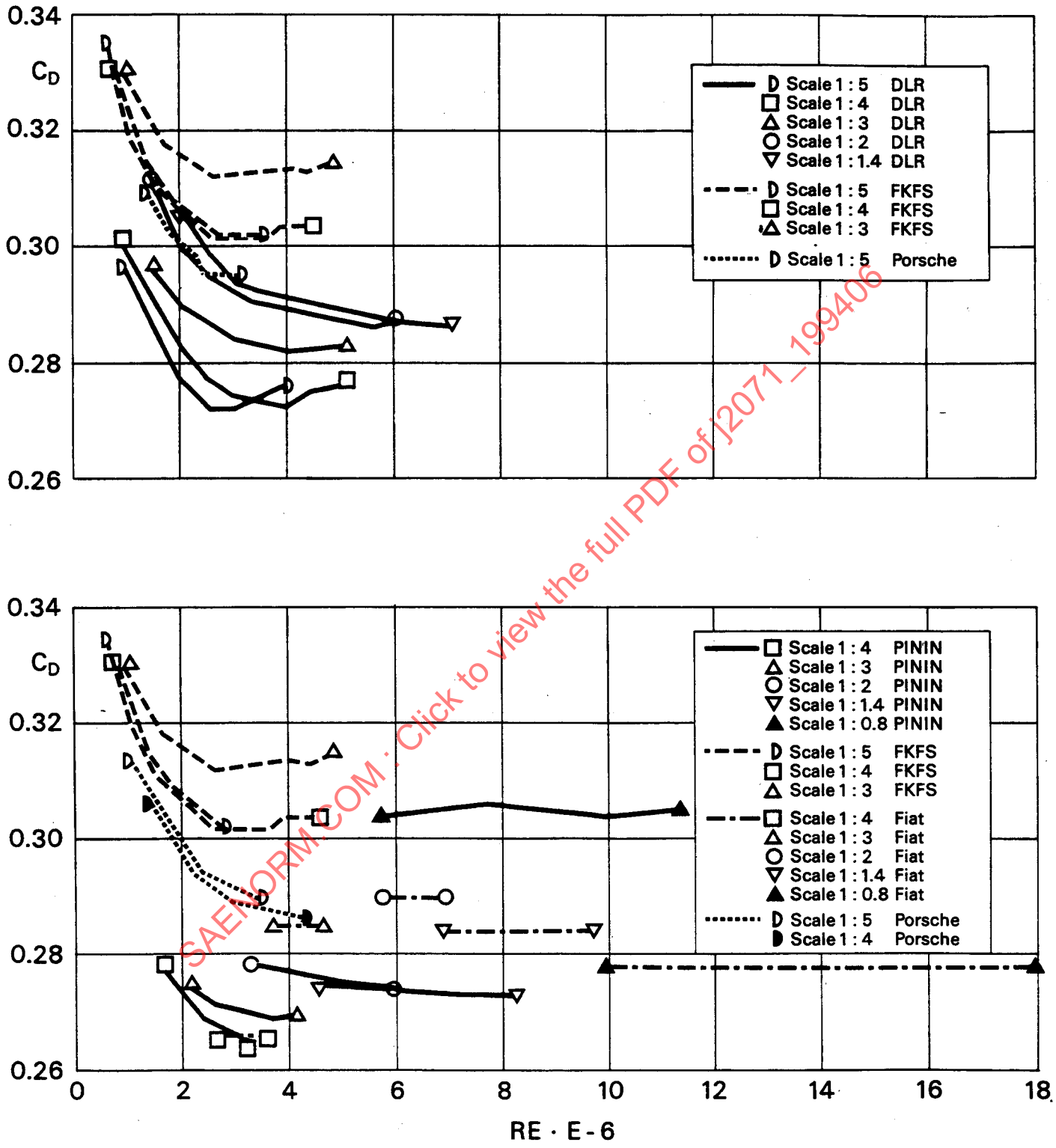

FIGURE 35—DRAG COEFFICIENTS OF MIRA NOTCHBACK MODELS

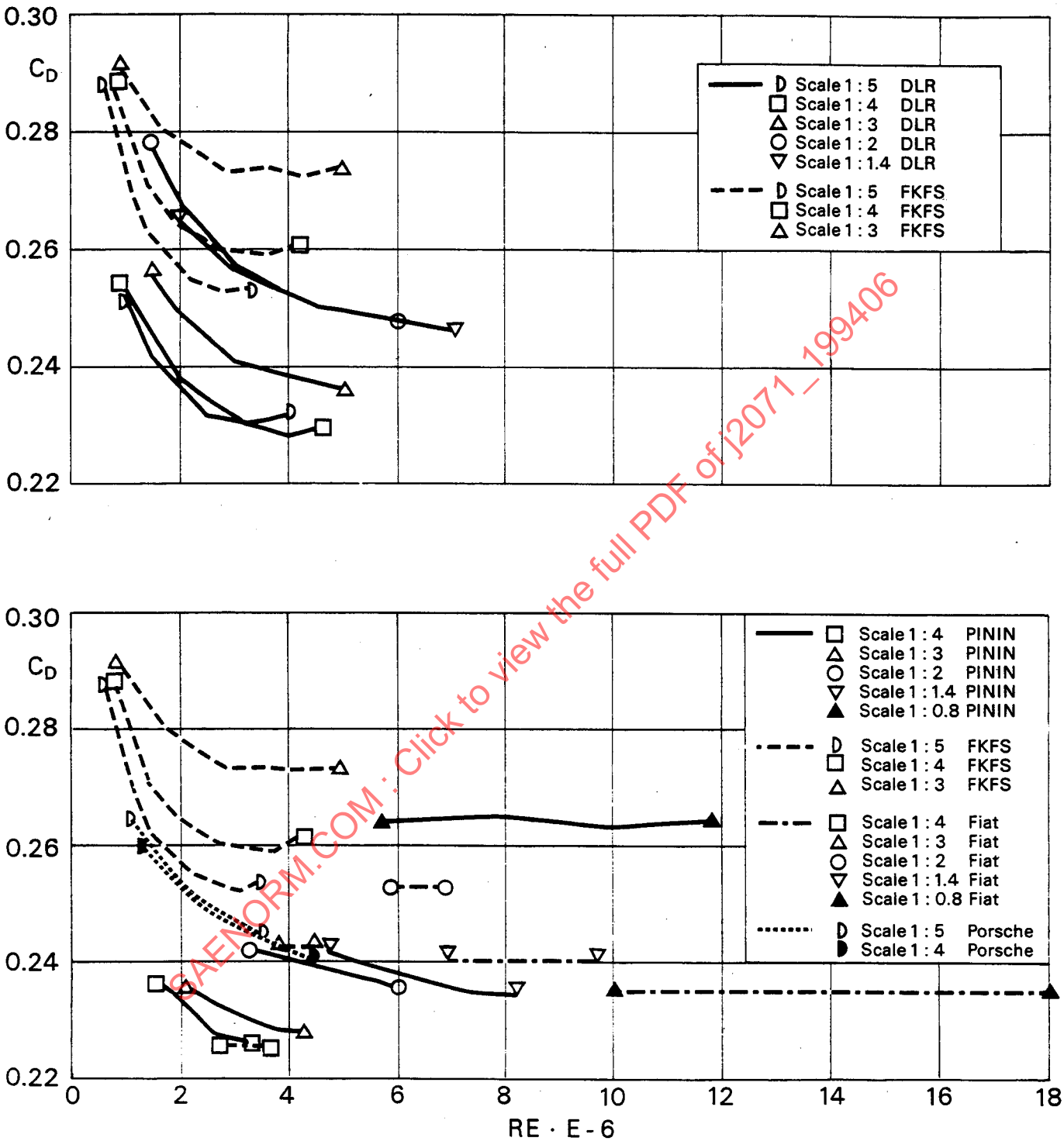

FIGURE 36—DRAG COEFFICIENTS OF MIRA FASTBACK MODELS

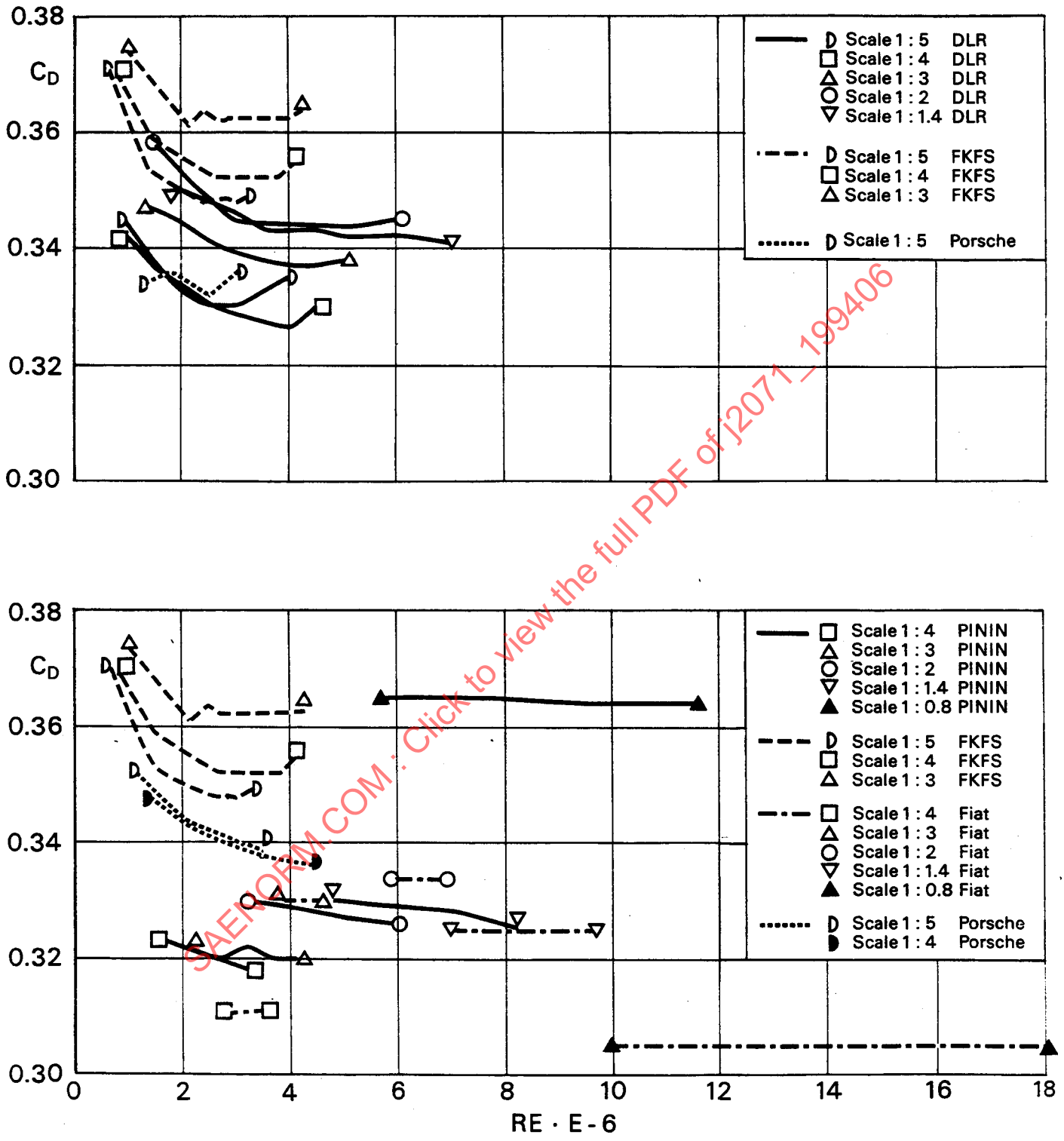

FIGURE 37—DRAG COEFFICIENTS OF MIRA STATION WAGON MODELS

Figure 38 shows that misleading results may be obtained if the tests are conducted at one wind speed only. The tests show that the differences in C_D become smaller with increasing Reynolds number.

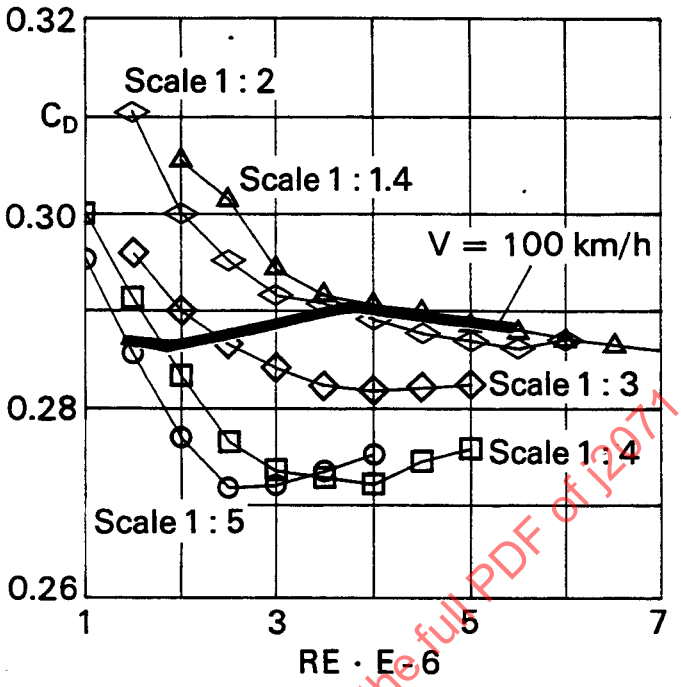

FIGURE 38—DRAG COEFFICIENTS OF MIRA NOTCHBACK MODELS IN DLR WIND TUNNEL

Under the restrictions discussed, the influence of blockage ratio on C_D in different wind tunnels is shown in Figure 39. For each model, the C_D value measured at the highest attainable Reynolds number or if possible at $Re = 9 \cdot 10^6$ is selected. In Figure 39 the value, at $A/A_N = 5\%$, is arbitrarily taken as reference.

6. *Conclusions From the Experiments*

6.1 Interference Effects in General—For many years it has been thought that, for blockage correction, an open jet wind tunnel should be treated mathematically in the same manner as a closed test section. This is true, but under the term "blockage effects" are often included all interference effects, which could occur in an open test section. It is not surprising, then, that corrected data often do not improve the agreement between data measured in different wind tunnels with the same model.

Theoretically, it can be shown that the blockage corrections of open jet test sections are of opposite sign and much smaller in magnitude than in closed test sections. Therefore, corrections are often omitted. But, unfortunately, possible additional interference effects beside blockage can compensate for, or even overshadow, blockage effects. Therefore, it seems necessary to evaluate and to distinguish between the different interference effects and to apply a correction procedure to the measured data, even though the resulting drag change might be zero for certain model tunnel configurations.

The additional interference effects are caused by the different test section components, in the way they are designed and tuned (nozzle, collector, plenum chamber). In a strict sense, the effects are a consequence of blockage and are caused by the model placed in the test section, but they cannot be ascribed to blockage. This shall be illustrated by an example taken from interference effects in closed test sections where corrections are applied on a routine basis (SAE J1913 DRAFT):

The flow in a closed test section is constrained by the walls around the body and the wake of a vehicle and continuity of flow requires an increase of airspeed around the model. This effect is commonly termed "blockage". Additionally, due to the displacement of wake fluid in a constrained flow, a horizontal pressure gradient over the model is created, which is termed "horizontal or wake buoyance effect". Clearly, the latter effect is a consequence of blockage, but it does not belong to blockage and it is, therefore, treated mathematically different in the correction procedures.

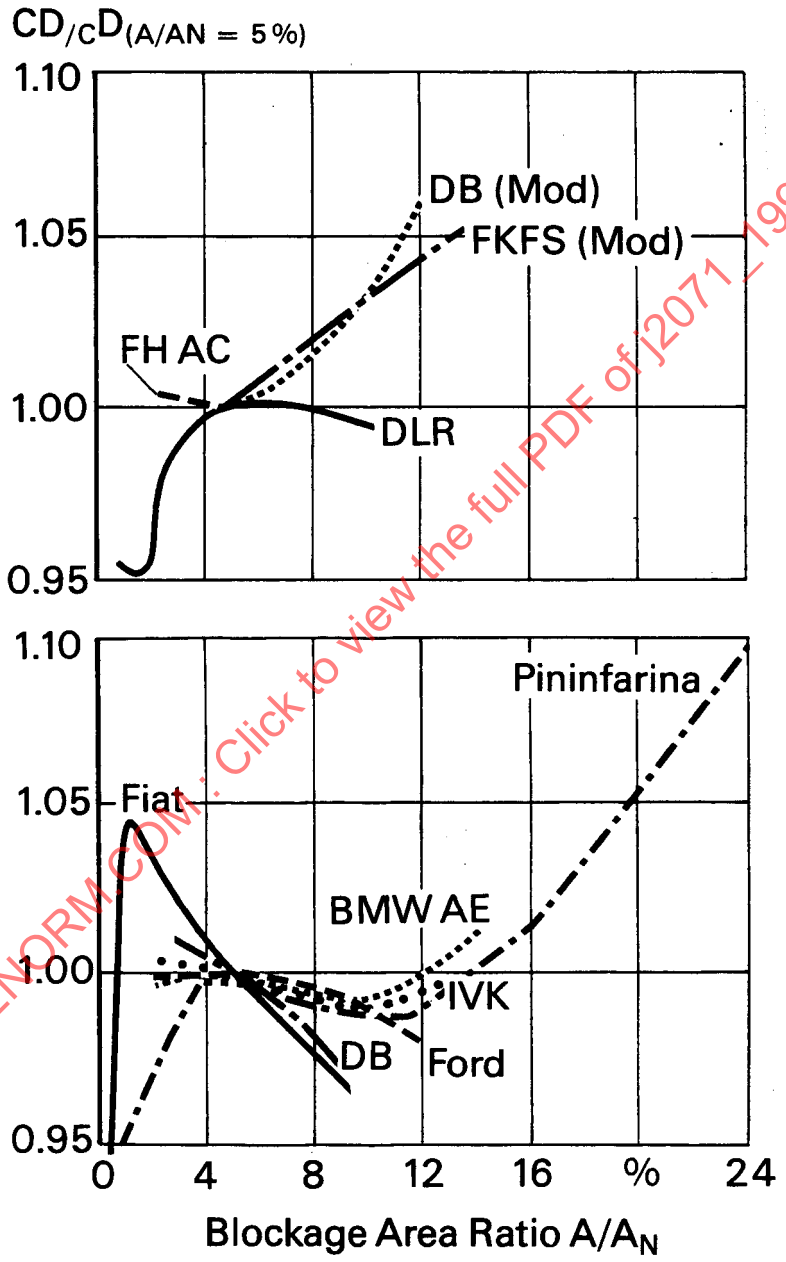

FIGURE 39—MEAN RELATIVE DRAG COEFFICIENTS OF MIRA MODELS IN DIFFERENT WIND TUNNELS AS A FUNCTION OF BLOCKAGE AREA RATIO (C_D AT A/A_N = 5% IS ARBITRARILY TAKEN AS REFERENCE)

6.1.1 BLOCKAGE EFFECTS—Before the interference effects of the different test section components are discussed as a consequence of blockage, it should be understood how a jet behaves with a model present, that is to say, how a jet alone experiences blockage.

When a model is measured in an open test section, the jet, which is of finite dimensions, behaves slightly different to a jet of infinite extent.

In order to fulfill the boundary condition, the static pressure along the boundary streamline of the jet has to be constant and equal to the ambient pressure (pressure in the plenum chamber). Due to the displacement of flow around a model, the jet will be arched and the static pressure of an infinitely large jet tends to be lower at the same distance from the model compared to a finite jet. Thus, in order to balance the ambient pressure, the curvature of the streamlines has to increase in the latter case. A consequence of the additional streamline curvature at the boundaries is that the jet expands, and the area between model and jet boundary is increased. Continuity of flow then requires a decrease of velocity around the model and a lower drag coefficient will be measured.

This effect is termed "blockage effect" and should not be confused with the other interferences. Blockage correction is a pure velocity correction and should be applied to the q-measurement of the reference data of the tunnel.

6.1.2 ADDITIONAL INTERFERENCE EFFECTS—Beside blockage, the main interference effect in an open jet wind tunnel can be expected from the flow collector at the end of the test section. Depending on the length of the test section, the measuring position, and the design of the collector components, different interference effects are experienced. They can be minimized by suitable tuning of the collector, but in a tunnel where, due to space, certain limitations are imposed, corrections seem to be inevitable.

The cross section area of a collector is bigger than the area of the nozzle (the area ratio of both cross sections varies between 1.1 and 3.0 for the wind tunnels in operation). The reason for this enlargement is due to the fact that a shear layer is discharged from the trailing edge of the nozzle. Due to turbulent mixing, the shear layer grows in width while travelling downstream and the velocity in the shear layer decreases towards the outer region. Although the potential core of the jet, where the velocity is equal to the velocity measured at the nozzle, decreases in size downstream, the overall width of the jet increases. Depending on the test section length, and, thus, on the growth of the shear layer, the area ratio of collector and nozzle should be adapted. Thus, the collector area should be sufficiently greater than the nozzle area to avoid accelerating the jet core velocity as the jet enters the collector.

The shear layer also has the property of entraining fluid from the surrounding plenum chamber as well as from the potential core of the jet. As the plenum chamber is usually a closed environment, entrainment flow is branched off the jet and a dividing streamline between the recirculation flow in the plenum chamber and the jet flow can be assumed. This dividing streamline is located somewhere inside the shear layer.

A collector cross section area, which is not adjusted to the jets cross section area, will curve the dividing streamline because this streamline has to terminate in a stagnation point at the leading edge of the collector. Due to the varying streamline curvature in the downstream direction, a positive longitudinal pressure gradient is superimposed on the jet, and a model and its wake penetrating this area will experience a reduced drag force.

Furthermore, depending on model size, the stagnation point at the collector might be shifted in comparison to an empty test section and; therefore, a different pressure gradient is created.

If, for instance, models of increasing scale are tested in an open test section, the curvature of the dividing streamline in the proximity of the collector will be increased because the stagnation point is moved further to the outer portion of the collector. Consequently, the pressure gradient in the jet is increased and the drag force is decreased. If the model size is further increased, the expansion of the jet at the model location interferes with the surrounding plenum chamber and acceleration of flow takes place at the collector's entrance. A pressure gradient of opposite sign is created and the measured drag force on the model is now increased.

It is obvious that these effects depend on the dimensions of the plenum chamber, the test section length, and the collector's area. The extreme case is reached when the plenum chamber assumes the shape and dimensions of the nozzle. Indeed, the closed test section type of flow is then attained. But even for an infinitely large plenum chamber, acceleration of flow can occur at the entrance to the collector. This is the case when the expansion of the jet, due to blockage, becomes appreciably larger than the dimensions of the collector. However, all interference effects of the collector will vanish for wind tunnels with an infinitely long test section or, in other words, when the superimposed pressure field of the collector does not penetrate into the wake of the model.

If one assumes a vehicle in a wind tunnel of variable test section length, a qualitative drag curve can be drawn considering collector effects only (Figure 40). The same kind of tendency, or rather its mirror image, is revealed if, for a given open test section, an infinitely small model is successive increased in scale (Figure 41).

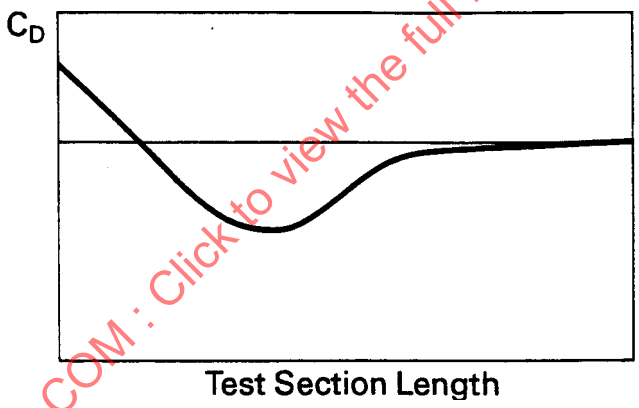

FIGURE 40—QUALITATIVE DRAG CURVE VERSUS TEST SECTION LENGTH CONSIDERING COLLECTOR EFFECTS ONLY

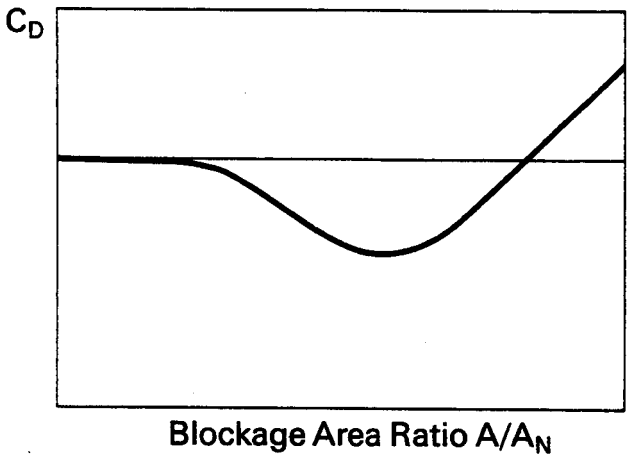

FIGURE 41—QUALITATIVE DRAG CURVE VERSUS BLOCKAGE AREA RATIO CONSIDERING COLLECTOR EFFECTS ONLY

6.2 Theoretical Interpretation of Experiments in Sections 3 and 4

6.2.1 FLAT PLATE MEASUREMENTS—The qualitative description of the interaction of the different test section components, can be illustrated by some drag measurements on flat plates. The plates were of different sizes and were measured in different positions inside the test section. The measurements were taken in the wind tunnel of Pininfarina and are described in Section 5. They comprise the most comprehensive data set for evaluating interference effects in open jet test sections.

In Figure 42 the drag coefficient C_D is shown as a function of the blockage ratio $C_D \cdot A/A_N$. The parameter of the different curves is the measuring position with respect to the center of the turntable, of the plates inside the test section. The area designated by A is associated with blockage and the superimposed effect of a shifted stagnation point at the leading edge of the collector. As expected, the drag coefficient decreases with increasing blockage ratio and this is most evident in the far downstream position of the plates. The influence of the collector is rather moderate in this area and becomes eventually more important in the area designated by B, the so-called "transition region". Blockage and horizontal buoyancy effects are fully compensated in this domain and a flat drag curve with increasing blockage ratio is revealed. In the third area, C, the collector becomes dominant and overrules all other interference effects. The flow is highly accelerated at the collector and the drag coefficient again increases. This is most obvious for the far downstream position of the plates where, due to acceleration of flow, the drag gradient can be nonlinear.